RESEARCH ARTICLE

ESPL **WILEY**

Decay of ignimbrite fairy chimneys of Arizona's Basin and Range Province, USA

Ronald I. Dorn [ORCID]

School of Geographical Sciences and Urban Planning, Arizona State University, Tempe, Arizona, USA

Correspondence
Ronald I. Dorn, School of Geographical Sciences and Urban Planning, Arizona State University, Tempe, AZ 85287-5302, USA.
Email: ronald.dorn@asu.edu

Abstract

Fairy chimneys of ignimbrite are well studied in Cappadocia in central Anatolia, Turkey. The ignimbrite landforms of Arizona's Basin and Range, USA, in contrast, remain relatively unexplored in geomorphic scholarship, despite decades of geological research on the characteristics of the ignimbrites themselves. This research focuses on the rock-decay processes that modify Arizona's Basin and Range fair chimneys. Dissolution of glass and groundmass, measured along joints using digital image processing of back-scattered electron microscope imagery, reveal a $3\times$ higher porosity than inside the rock interior. This method also measured a 3-4$\times$ increase in dissolution near the base of the chimney compared with the rock interior, leading to notch development that promotes chimney mass wasting and subsequent ballistic impacts. Epilithic organisms studied with electron microscopy both enhance rock decay and promote case hardening. These observations are consistent with prior understanding of how fairy chimneys evolve over time: columnar joints exposed on cliff faces experience enough decay to allow erosion of joint material, this erosion separates the chimney from the rock face and notch development near the chimney base promotes mass wasting. The rock-decay processes studied here likely operate on very different timescales. Mass wasting events leading to ballistic impacts occur at observable timescales. Varnish microlamination dating, using ultrathin sections of rock varnish formed on fairy chimneys, indicates that the case hardening of the top of fairy chimneys are much more stable than the sides; the tops last experienced surface detachment during the early Holocene, as opposed to the sides that experienced flaking throughout the late Holocene. The timescale of basal notch development is not known, with the exception that the very surface of notches erode at rates too fast to accumulate rock varnish. The timescales of epilithic organisms enhancing rock decay and dissolution of columnar joints are not known.

KEYWORDS
case hardening, columnar jointing, detachment, dirt cracking, erosion rate, flaking, weathering rind, welded tuff

1 | INTRODUCTION

Ignimbrite or ash-flow tuff results from explosive silica-rich volcanic eruptions. Deposition occurs in a variety of settings: eruption outflows beyond the source caldera before its collapse, intracaldera ignimbrites as the caldera collapses and caldera-filling ignimbrites after caldera collapse (Best et al., 2013).

Geomorphic landscapes developed on ignimbrite occur widely and produce a variety of landforms. These landforms include bornhardts or domed inselbergs (Campbell & Twidale, 1991), talus flatirons (Oh et al., 2020), tafoni (McBride & Picard, 2000), case hardening (Klaer, 1993; McBride & Picard, 2000; Paterno, 1999; Waters, 1966), escarpments (Skotnicki & Ferguson, 1995), slickrock (Larson et al., 2020), cliff faces (Dorn, 2018), pediments (Jeong

et al., 2018; Larson et al., 2020) and columnar forms—the focus of this research.

No definitive terminology exists for columns composed of ignimbrite. They have been called 'hoodoos' in Argentina (Aguilera et al., 2017), 'erosional columns' in the Chiricahua Mountains of Arizona (Hall, 1998), 'exposed columns' in Valles Caldera in New Mexico (Self et al., 2022), 'pinnacles' in City of Rocks State Park in New Mexico (Mueller & Twidale, 1988) and 'fairy chimneys' in Cappadocia, Turkey (Emre & Guner, 1988; Pasquare, 1968). Increasingly, however, the term fairy chimney is being adopted to describe ignimbrite columnar forms observed outside of Cappadocia, including Brazil (Pereira, 2019), Morocco (Bouzekraoui et al., 2018), Serbia (Valjarevic et al., 2015), Peru (Sparavigna, 2011), Azerbaijan (Anjbaran, 2018) and Iran (Kaljahi & Birami, 2015). Thus, 'fairy chimney' is the term employed here.

Columnar jointing is thought to be a first key step in the development of a fairy chimney (Pallister et al., 1997; Self et al., 1996). As tuff cools, columnar joints develop at right angles to cooling surfaces from a decrease in volume due to cooling; this then generates tensional stresses (Hetényi et al., 2012). Columnar joints can be planar or curvilinear (Pallister et al., 1997).

A second key is exposure of the ignimbrite columnar joints along a cliff face, aided by such processes as the development of drainages associated with regional base level changes (Dogan et al., 2019). An example of this second step comes from the fairy chimneys of Cappadocia, Turkey (Kuzucuoglu, 2019; Scoon, 2013; UNESCO, 2022), where Quaternary fluvial incision of the Melendiz River Valley lowered base level and led to the development of drainages into ignimbrite plateaus (Dogan et al., 2019). Canyons eroding back into ignimbrite plateaus expose a sequence of durable and nondurable ash-flow tuffs occasionally interbedded with lacustrine deposits (Deniz & Topal, 2021). The fairy chimneys then separate from the cliff face, as erosion removes material from decayed columnar joints (Sarikaya et al., 2015).

A third key to fairy chimney formation is sufficient material strength not collapse under its own weight (Hall, 1996; Pallister et al., 1997). Rock properties are a critical control on bedrock landforms in general (Duszyński et al., 2021), where rock strength is a measure of the pulling force required to rupture the rock, and durability is of the rock's ability to withstand rock-decay processes; rock decay is the term preferred here rather than 'weathering' for reasons explained elsewhere (Hall et al., 2012). Both strength and durability are measured in a variety of ways, in the laboratory and in the field (Ahmad et al., 2017). Field-based electrical resistivity and needle penetration, for example, established basic engineering geological properties of the Cappadocia fairy chimneys (Aydan et al., 2022; Kahraman, 2022), which appear to have lower strength (Aydan et al., 2022; Kahraman, 2022) than Arizona ignimbrites studied in Chiricahua National Monument (Dombroski & Fodor, 2019; Hall, 1993).

A fourth key to fairy chimney development is a slow enough rate of rock decay to allow vertical or near-vertical slopes to persist. These decay rates, however, vary a lot (Dincer & Bostanci, 2019; Erguler, 2009; Garvia-Valles et al., 2003; Municchia et al., 2018), because different ignimbrites vary in their susceptibility to different decay processes (Moon, 1993); this variability led to a broad classification into durable and nondurable ignimbrites, where development of

columnar towers requires sufficient durability to maintain the near-vertical side slopes (Moon, 1993). The Cappadocia fairy chimneys, for example, start with a cap of durable ignimbrite that slowly reduces in size to nothing, leaving behind nondurable tuffs that then erode quickly after removal of the caprock (Sarikaya et al., 2015; Topal & Doyuran, 1997).

The focus of this research rests on the role of rock decay at different stages in the development of fairy chimneys in Arizona. Scholarly research on fairy chimneys in Arizona is nascent with only limited study in the Chiricahua Mountains (Enlows, 1955; Hall, 1996, 1998; Pallister et al., 1997) where research focused on the role of jointing, as well as mass wasting. Unlike the Cappadocia (Dincer & Bostanci, 2019; Erguler, 2009; Garvia-Valles et al., 2003; Municchia et al., 2018), no scholarship exists on rock-decay processes on the fairy chimneys in Arizona.

Arizona's fairy chimney are found mostly in the Basin and Range physiographic province of Arizona, USA, selected as a study region because of the presence of extensive areas of ignimbrite (Best et al., 2013). This province has considerable overlap with the Sonoran Desert, where aridity promotes weathering-limited landscapes and extensive exposures of bare ignimbrite bedrock landforms including: classic pediments (Larson et al., 2014; Larson et al., 2020), domed inselbergs (e.g., 33.4645, −113.3612; 33.3587, −114.0719), slickrock of the sort typically studied in sandstone (Oberlander, 1977) and ubiquitous tafoni and case hardening on these forms. Fairy chimneys are common ignimbrite landforms that generate spectacular landscapes throughout the Basin and Range of Arizona (e.g., Figure 1).

Six linked investigations carried out here were designed to understand better the role of rock decay in the development of fairy chimneys in ignimbrites in Arizona's arid Basin and Range. Figure 2 helps explain these linkages graphically. Figure 2a highlights the step of chimney separation from the main rock mass—studied here using electron microscopy to measure dissolution and other decay processes in columnar joints. Figure 2b highlights rock decay at a notch near the base of a fairy chimney—also studied through electron microscopy. Instability of the chimney base promotes mass wasting of column pieces and entire columns (Figure 2d) that then leads to ballistic impacts against adjacent chimneys—analysed here through field surveying and electron microscopy. Figure 2c presents the side of a chimney experiencing both case hardening of surfaces and decay via lichens and fungi—also studied using electron microscopy. The last investigation involves the use of varnish microlamination (VML) dating to provide insight into rates of rock-surface spalling, resulting from these decay processes.

2 | METHODS

2.1 | Study site selection

The Basin and Range Province (BRP) of Arizona (Figure 3) is part of a larger region in western North America that experienced explosive silicic volcanism from 36 to 18 Ma, with more than 30 super-eruptions of volumes greater than 1000 km^3 (Best et al., 2013). Forty-two exposed calderas had diameters greater than 60 km. In the BRP of Arizona, ignimbrites comprise all or part of over 40 desert mountain ranges from dacitic, trachydacitic and rhyodacitic eruptions (Best
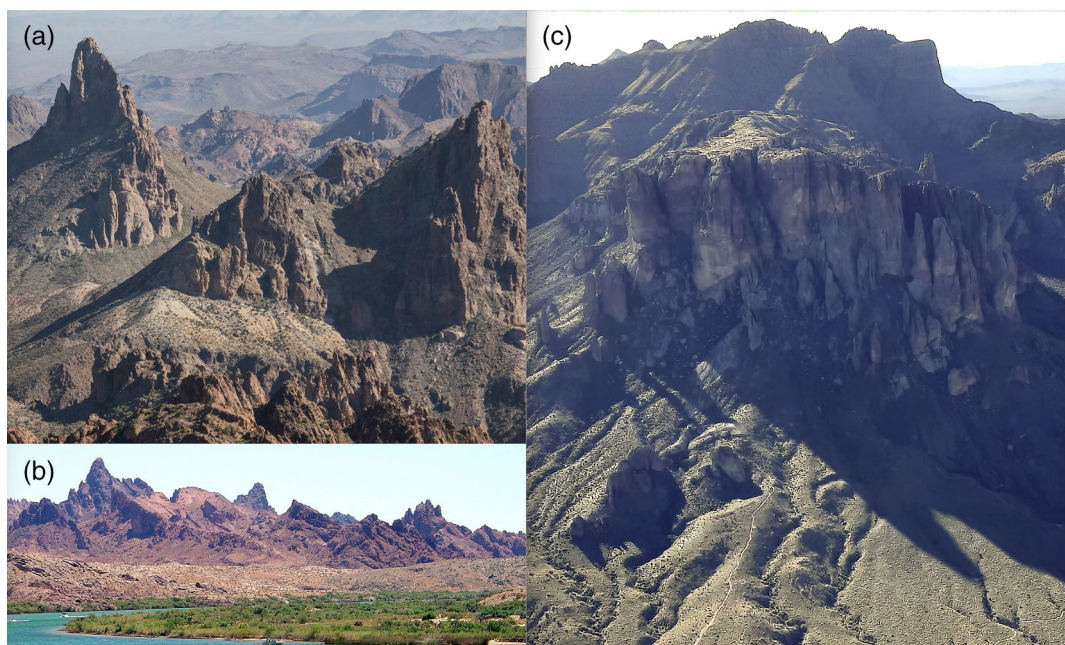
FIGURE 1 Examples of ignimbrite landscapes with fairy chimneys in the Basin and Range Province of Arizona. (a) From the top of the Kofa Mountains (33.3446, −114.082). (b) The Needles (34.6749, −114.4523) along the Colorado River where the geological literature only mentions these columnar forms in passing (Howard et al., 2013; Sherrod & Tosdal, 1991). (c) The Superstition Mountains (33.4481, −111.4602) with hiking trails providing scale. Note that as fairy chimneys separate from the cliff, they decrease in height as a result of mass wasting events.

FIGURE 2 Graphical explanation of the different rock-decay investigations carried out on Sonoran Desert fairy chimneys. (a) Dissolution within columnar joints (down arrow) thought to promote chimney separation from a rock mass. (b) Rock decay at notches along the base (side arrow) of chimneys hypothesized to promote mass wasting. (c) Epilithic organisms like fungi are hypothesized to both case harden (CH) and promote spalling (S) of notches (arrow) along base of fairy chimneys. (d) The rate at which chimney surfaces become unstable was studied by varnish microlaminations on the sides and tops of chimneys. Ultimately, instability due to notch growth (arrow) promotes mass wasting of blocks (or entire chimney) to become talus or impact adjacent chimneys. (CH) Back-scattered electron (BSE) micrograph of case hardening (sampled at CH in image c) caused by fungi (f) holding in place the decayed remnants of the underlying rock. (S) Once fungi detach, loose material underneath erodes and continued spalling occurs along the chimney basal notch as illustrated by jagged fractures in this BSE image (sampled at S in image c).
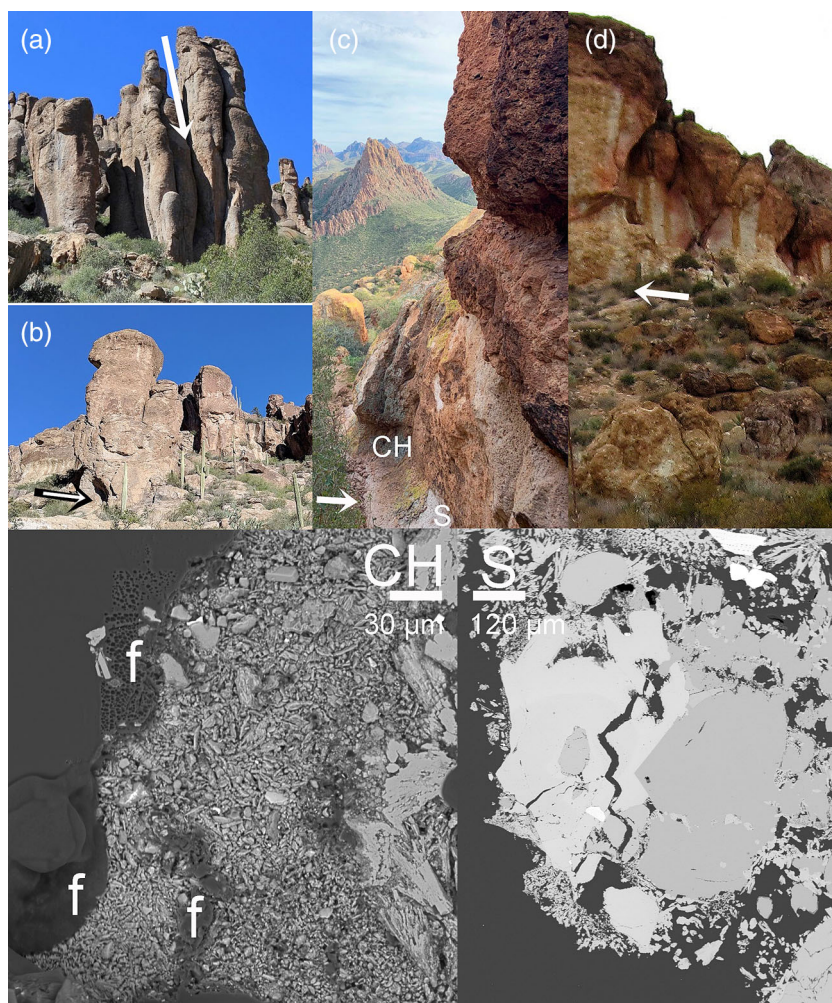
FIGURE 3 The study area is the portion of the Goldfield-Superstition Volcanic Province (Dombroski & Fodor, 2019) resting within the Basin and Range. This includes the main Superstition cauldron and associated smaller Black Mesa, Florence Junction, La Barge Canyon, Haunted Canyon and Willow Springs cauldrons (Royse et al., 1971; Stuckless & Sheridan, 1971); modified from Dombroski & Fodor (2019).

et al., 2013). The conceptual tectonic thinking is that these silicic eruptions resulted when a flat subducting plate (during the ∼70–40 Ma Laramide Orogeny; Sales, 1968; Yonkee & Weil, 2015) started to steepen again ∼38 Ma into a more typical subduction zone; this transition in subduction zone angle may have injected a high influx of mantle magma into the continental crust (Best et al., 2013). All of the ignimbrite areas (Best et al., 2013) in Arizona have an abundance of fairy chimneys, but the Goldfield-Superstition Volcanic Province (Dombroski & Fodor, 2019) (Figure 3) was selected for the logistical reason of access via dirt roads and trails. Also, all of the sites in the Goldfield-Superstition Volcanic Province have similar climate, biota and lithology but do face different directions allowing an investigation into the role of aspect on epilithic organisms.

The particular study sites selected for sampling (e.g., Figures 4–6) also display a wide variety of features that are beyond the scope of the research question. These features include tafoni, alveoli, slickrock, bornhardts or domed inselbergs, pediments and other forms. An encyclopaedic investigation of all the various potential linkages between rock-decay processes and these forms is beyond the scope of this study. Rather, the sampling employed here focused on trying to capture insight into: decay processes in joints to help separate a chimney from the main rock mass; decay processes around the basal notch of a

fairy chimney that could promote mass wasting of the chimney; ballistic impacts of chimney mass wasting; and rates of surface loss along chimney sides and tops due to rock decay. The electron microprobe method used to analyse rock decay requires sample sizes less than a centimetre in the longest dimension, due to the nature of the instrument sample chamber. This small size permits the application of epoxy in the field to 'freeze' *in situ* relationships that might have otherwise been disturbed by sample removal. Sample removal typically involved gentle prying of the epoxied material with fingers; a rock hammer was only needed in a few locations.

Fairy chimneys (e.g., Figures 4–6) are ubiquitous within the Goldfield-Superstition Volcanic Province (Dombroski & Fodor, 2019). Two of the most spectacular areas are Martinez Canyon (Figure 4a) and around Weaver's Needle (Figure 4b). Both areas offer ideal collection sites to examine rock-decay processes potentially involved in separating fairy chimneys from the main cliff face (circles identified by arrows in Figure 4). Weaver's Needle (Figure 4b) itself is rhyodacite lava, but joint was sampled in an ash-flow tuff.

Figure 5 compiles other fairy chimneys in the Goldfield-Superstition Volcanic Province that offer accessible sites to collect samples to analyse rock decay using electron microscopy techniques. Figure 5a in the Martinez Canyon area shows a location where a more
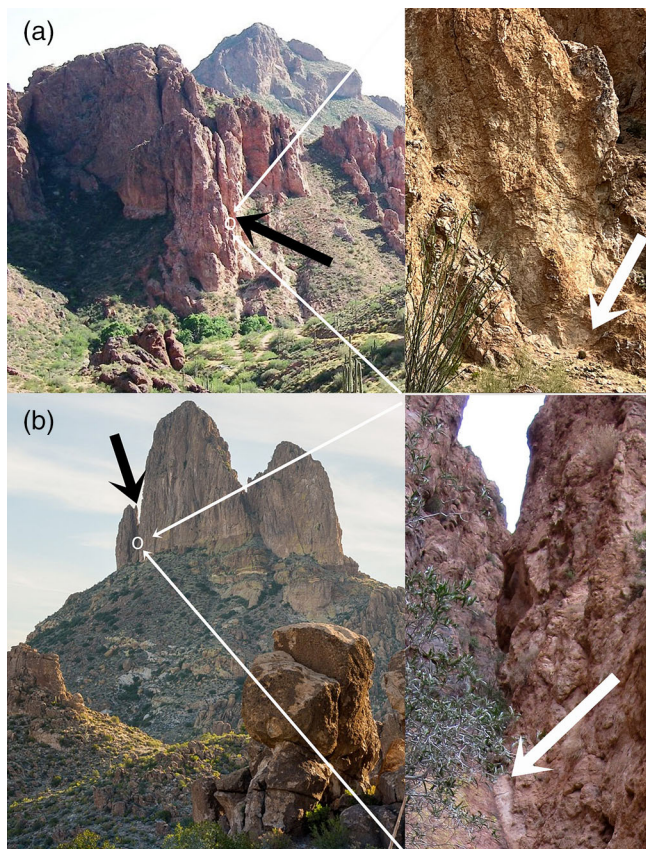
FIGURE 4 Examination of the separation of fairy chimneys from the main ignimbrite mass required collection of samples from the bottom of eroded columnar joints. Samples were collected at circles identified by arrows at Martinez Canyon (A, 33.1672, −111.1556) and Weaver's Needle (B, 33.4331, −111.3704). Close-ups identifying specific sampling spots are on the right; the fairy chimneys in (a) are about 50 m tall. Weaver's Needle in (b) is about 300 m above the surrounding topography.

resistant tuff unit caps columns. Here, rather than separate to form distinct fairy chimneys, these columns experience rock falls or toppling before they develop distinct separate chimneys. The white arrow in Figure 5a indicates the collection site to examine processes involved in the lack of chimney separation. Figure 5b shows fairy chimneys in the Bulldog Canyon area that are being undercut at their base by enhanced rock decay at a notch; the white arrow in Figure 5b is a collection site. Figure 5c in the Weaver's Needle area is a topple (upper arrow indicates collection at the topple contact point) that also displays case hardening (lower arrow identifies sampling spot to evaluate the impact site). Figure 5d at the head of Martinez Canyon is sometimes called 'the chipmunk god' and displays both grooves and case hardening associated with lichen growth (arrow indicates sampling spot).

In situ cosmogenic nuclides provide insight into rates of surface erosion (Sarikaya et al., 2015), including mass wasting events. In contrast, this study's focus rests in understanding the role of rock decay in Arizona's fairy chimney development; a more appropriate—but less precise—method to measure rates of rock decay involves VML dating (Liu & Broecker, 2007, 2013). Unlike cosmogenic nuclides, a numerical dating method, VML is a calibrated dating method. VML sequences are analysed on landforms with a numerical age such as a regressional palaeolake shoreline or a landslide deposit dated by radiocarbon

analyses on buried wood. These numerical ages, provided by different dating strategies, were then be used to calibrate VML patterns in a climatic region. In the case of Basin and Range, a calibration for the Holocene (Liu & Broecker, 2007) has been independently verified with additional calibration points in the Sonoran Desert (Dorn, 2014). Unlike numerical methods that have measurement-based uncertainties, the VML method's uncertainties rest in the broad timescale of its calibration intervals. Thus, instead of having a symmetrical plus–minus, the uncertainty would be in an interval of hundreds to a few thousand years between calibration points. More insight into the VML method is presented later, as this section focuses on sampling.

The area around Weaver's Needle (Ferguson & Skotnicki, 1995) contains a labyrinth of fairy chimneys appropriate to obtain rough estimates of rates of surface detachment from rock decay using VMLs. Much like the high cost of cosmogenic nuclide dating limits the number of samples feasibly analysed (e.g., Sarikaya et al., 2015), approximately 3.5 weeks of lab time needed to make the analysed VML ultrathin sections analysed here limits the total number of samples feasibly studied.

After gridding an aerial photograph into 144 (12 × 12) even-area cells, two rolls of two six-sided die identified 10 cells for collecting surface samples for VML dating. The nearest fairy chimney to the centre of these 10 areas (that the author was able to climb to the top) was sampled on the top and exposed sides. Thirty rock chips sampled from both chimney tops and sides assessed their geomorphic stability, because VML provides a minimum-limiting age for when a surface last detached, in this case via millimetre-scale flaking. The criteria for selecting the location for chipping was locations that largely lack fungi and lichens, because these epilithic organisms secrete acids that erode the VMLs (Dorn, 2014).

2.2 | Electron microprobe analyses of dissolution in joints and notches

A JEOL electron microprobe is a versatile tool to analyse rock decay in that it acquires different types of imagery and elemental analyses at a micron scale. For all samples, epoxy was first applied to surfaces in the field prior to collection; this was to preserve *in situ* relationships that can be disturbed by the removal of rock surfaces. Samples were then placed in an epoxy mould suitable for a microprobe stage. Cross-sections were then polished with the final step being 0.1 μm aluminium paste. Two electron microprobe techniques provide imagery and elemental chemistry: back-scattered electron (BSE) imaging and qualitative analysis of energy-dispersive spectra (EDS) (Reed, 1993). BSE imagery facilitates the identification of dissolution (as black porous areas that were quantified using digital image processing as explained below), as well evaluation of mineral and glass alteration. EDS determines the elemental composition of specific points or areas.

One part of the investigation into joint decay and notch decay involved qualitative observations using EDS and BSE to understand the nature of processes at Figures 4 and 5. Quantification of the amount of dissolution in joints (Figure 4) and at notches at chimney bases (Figure 5b) required BSE images, because black areas indicate porosity—that can be analysed through digital image processing using a method detailed elsewhere (Dorn, 1995; Dorn & Brady, 1995) that quantifies the per cent porosity.
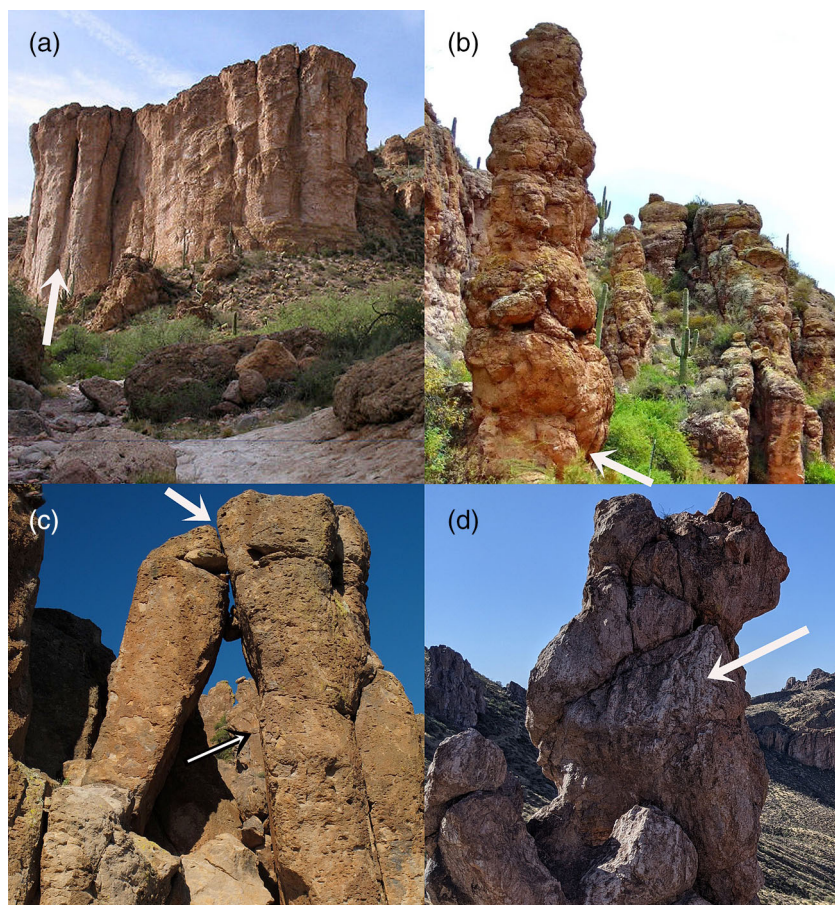
FIGURE 5 Well photographed features that exhibit different processes of fairy chimney development in the Goldfield-Superstition Volcanic Province. The text provides details on sites and reasons why samples were collected at the arrows in (a) 33.1620, −111.1630, (b) 33.4777, −111.5444, (c) 34.4192, −111.3745 and (d) 33.1693, −111.1370. The vertical scale of these forms is (a) 20, (b) 15, (c) 8 and (d) 11 m tall.

FIGURE 6 Ten randomly selected locations (arrows) in the Weaver's Needle fairy chimney labyrinth (33.429, −111.370) sampled for VML dating of both chimney sides and top.

In brief, the quantitative method (Dorn, 1995; Dorn & Brady, 1995) applied here involves acquiring at least 1 000 000 μm^2 or 1 mm^2 of a sample at 1000× magnification. This is an area sufficient to characterize dissolution (Dorn, 1995; Dorn & Brady, 1995). Second, NIH ImageJ (https://imagej.nih.gov/nih-image/) contains algorithms to calculate mineral and rock porosity. In the case of the joint dissolution analysis, the cross-sectional area had the shape of a 1000 μm by 1000 μm square. In the case of the notch dissolution analysis, the cross-sectional area was 'cut out' digitally along the rock surface with the area being 5000 μm long and 200 μm deep in order

to understand the porosity of the very surface of fairy chimney. Three separate investigations in this study employed this method:

i. For the study of joint dissolution at Martinez Canyon (Figure 4a), 10 sets of paired samples were collected at the base of the joint. Each set consists of a surface sample a few millimetres across and then a sample from about 3 cm into the rock face. All 10 pairs come this location. The amount of dissolution within the joint and away from the joint can then be compared with an average, standard deviation and *p* value. The investigation of joint

dissolution at Weaver's Needle was qualitative, examining the nature of rock decay in electron microscope imagery collected where the joint had not yet eroded, but was present as decayed rock material at the circle in Figure 4b.

ii. For the study of notch development, Figure 5b shows a fairy chimney that has a distinct notch at its base. Similar basal notches occur commonly on fairy chimneys where soil has built up at the base. The soil line is where the top of the soil contacts the fairy chimney, with the idea that the capillary water in soil stays in contact with the fairy chimney much longer than exposed rock (Jessup et al., 2011). To test the hypothesis that basal notches result from enhanced rock decay near the soil line, dissolution was measured using the BSE digital image processing method at the notch and a metre above the notch. All 10 paired samples were collected from all sides of Figure 5b. The amount of dissolution at and well above a notch was then compared through the average, standard deviation and *p* value.

iii. A second study of notch development was conducted in response to a reviewer suggestion to quantify the ballistic impacts of mass wasting events, detailed in the next Section 2.3. The same fairy chimneys that experienced the ballistic impacts also had notches at their base. Paired samples of the notches of these 11 chimneys and 1 m above the notches were collected and analysed by the same method used for Figure 5b. However, instead of obtaining detailed paired samples for just one chimney, the paired samples were single pairings for the 11 chimneys that experienced ballistic impacts from the site detailed in the next Section 2.3.

2.3 | Ballistic impact investigation

A reviewer posed two questions regarding the mechanical impact of the mass wasting seen in the topple in Figure 5c: How frequent are these impacts? How large? To answer these questions, the area around Weaver's Needle (Ferguson & Skotnicki, 1995) hosted a survey of such impacts in a location with a particularly a high density of fairy chimneys: at Fremont Saddle (33.415, −111.365) on a slope averaging 18°. A randomly selected area in the centre of the slope 500 m × 250 m contains over 100 fairy chimneys. Working from one end of the study area to the other, every chimney was evaluated for the presence of rocks that fell against a fairy chimney until the count reached 100 chimneys. No chimney was skipped in this survey. Every topple, rock slide or rock fall that impacted a surveyed chimneys was measured for area of the rock-to-rock impact. Because rock varnish only forms on surfaces after the pulverized rock material had eroded away, and the time interval between impact and removal of pulverized rock is not known, the frequency question could was not addressed using the VML method discussed below. However, the number fairy chimneys that experienced ballistic impacts from fragments that fell against them could be counted and size of impact measured directly. Where possible, samples for electron microscope observations were collected from impacted areas.

2.4 | Fungi-lichen investigation

Another reviewer hypothesized that the hyphae of black fungi or lichens might offer important avenues for water penetration into chimney interiors and suggested an analysis to evaluate black fungi penetration on north-facing aspects. To conduct this investigation, the same Fremont Saddle (33.415, −111.365) fairy chimneys study area was investigated as in Section 2.3. The first 10 chimneys examined for ballistic impacts (see Section 2.3) were sampled on the north-facing side at height of 1 m above the chimney base, first applying epoxy and then removing about a centimetre square of the rock surface. These samples were then polished into cross-sections as in Section 2.2.

For each of these samples, a thousand micrometres of rock surface was then examined for evidence of fungal hyphae. The start of each 'transect' was at the middle of the sample, and 500 μm in each direction was evaluated for (i) presence of fungi or lichen on the surface of the rock face, (ii) presence of hyphae extending down into the rock into a fracture, (iii) length of the hyphae extending down the fracture and (iv) length of the fracture that can be longer than the hyphae. The result of this investigation can only provide a minimum estimate of the impact of these hyphae, because many fractures exist without hyphae. Such fractures could be abiotic in origin, or could be from a time when an epilithic organism existed, but then died off at some time in the past.

2.5 | VML dating

VML ultrathin sections that contained layering sequences suitable for analyses were made from 60 sections: three samples on a fairy chimney top and three samples on the sides of 10 randomly sampled fairy chimneys in Figure 6. In this site-selection process, the fairy chimney labyrinth in the Weaver's Needle area (33.429, −111.370) was gridded into cells, and 10 cells were randomly selected. The chimney closest to the centre of selected cells, that the author could physically climb, was sampled at the top and sides.

Multiple VML samples—many more than could be feasible prepared here—were taken from the top and the side for laboratory analysis. The criteria for collection following guidelines used in other VML studies (Dorn, 2014, 2016, 2018; Liu & Broecker, 2007, 2013); in brief, there are many confounding factors that can lead to rock varnish being unsuitable for VML dating, and the sampling strategies employed by these authors and used here maximizes the chance that the hours involved in sample preparation would yield a well-laminated cross-section suitable for analysis. The growth of black fungi and lichens dissolving laminations were the most common difficulties encountered in this VML study. Samples ended up being excluded during the polishing process when an area of laminated varnish could not be found between these acidic epilithic organisms. For example, of 20 rock chips placed in an epoxy mould from a chimney top, it typically took 10 to 12 polished chips to produce three suitable VML sequences. Sample preparation stopped after laboratory processing supplied three datable VML sequences from the top and sides of 10 chimneys. This limit was imposed by time 3.5 weeks of lab time to complete these VML samples.

The Holocene calibration developed by Liu and Broecker (2007) and subsequently tested with additional calibration points added for the Sonoran Desert (Dorn, 2014) provided age estimates of when sampled top and side surfaces last detached by millimetre-scale flaking. The VML Holocene calibration is based on 15 study sites that

were dated by independent means (Liu & Broecker, 2007). Examples of additional local Sonoran Desert calibration points are rock slides that crushed trees that were then radiocarbon dated, and the VML sequence came from the boulders resting on the dated wood (Dorn, 2014). The Holocene calibration consists of 12 diagnostic layering units produced during wetter climatic intervals spaced throughout the last 11 000 calendar years. These are black layers in the lamination sequence. The orange layers accumulated during intervening drier periods. Thus, a VML age can never be precise but providing only an approximate time for when the underlying surface last eroded and varnishing started.

Key limitations, however, exist with using this method: (i) three separate millimetre-sized samples that yielded a top and side VML age may or may not be statistically representative, and (ii) VML ages are always minimum limiting, because the bottom layer only starts to form *after* an erosion event, with a typical time lag being decades to a century in the study area (Dorn, 2014, 2016, 2018; Liu & Broecker, 2007, 2013). In essence, the purpose of this VML study was to provide insight into how long it takes rock decay to destabilize a fairy chimney surface in the study area.

3 | RESULTS

3.1 | Dissolution in columnar joints separating fairy chimneys from an ignimbrite cliff

Figure 4 shows fairy chimneys in the midst of separating from a cliff face. Although a variety of different processes could potentially be involved in this separation, dissolution was the process measured here by comparing dissolution in a joint to dissolution inside the unseparated rock. As noted earlier, 10 pairs of samples were collected from the joint in Figure 4a. Each pair was collected at the base of the joint—ringing it. Each set consists of a surface sample a few millimetres across and then a sample from about 3 cm into the unseparated rock face. An average and standard deviation of 10 paired samples yielded a threefold higher porosity of 23.38 ± 5.76% in the decayed joint, as opposed to inside the rock face of with 8.19 ± 4.30% dissolution. The difference is statistically significant at $p < 0.001$.

Figure 7 illustrates typical BSE images of what these joint samples look like. In all of the samples analysed, the same basic pattern occurred: multiple jagged parallel cracking throughout the joint area and substantial dissolution as indicated by the black (porous) areas.

Lower magnification BSE imagery (Figure 7) reveals that the bulk of dissolution occurs within the glass matrix between phenocrysts. Figure 8 illustrates this at higher resolutions. No matter whether the minerals are large phenocrysts or smaller minerals within the glass matrix, they appear to be experiencing much less dissolution than the
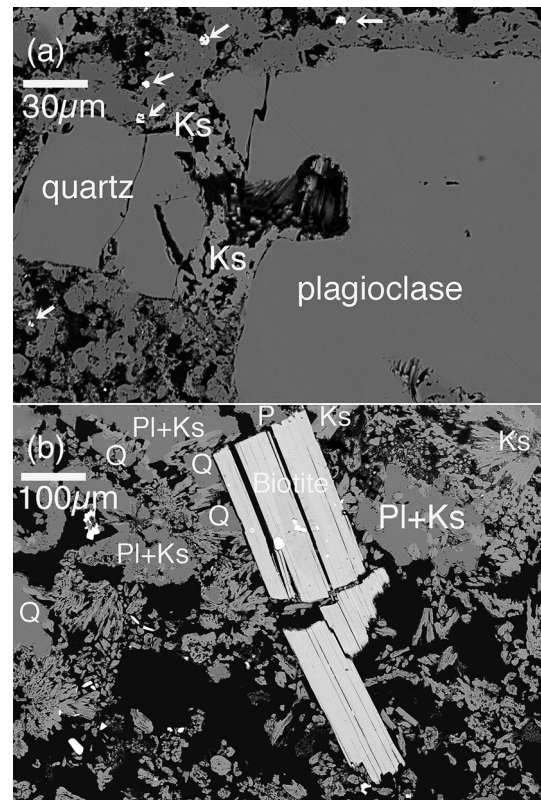

FIGURE 8 Glass dissolution appears to be much more extensive than mineral dissolution in BSE images of the joints, exemplified by the Martinez Canyon joint (image a from Figure 4a) and Weaver's Needle joint (image b from Figure 4b). Although some internal mineral dissolution does occur in plagioclase (Pl), orthoclase (Ks), quartz (Q), magnetite (arrows in image a) and biotite, the amount of porosity is much more extensive in the surrounding glass.
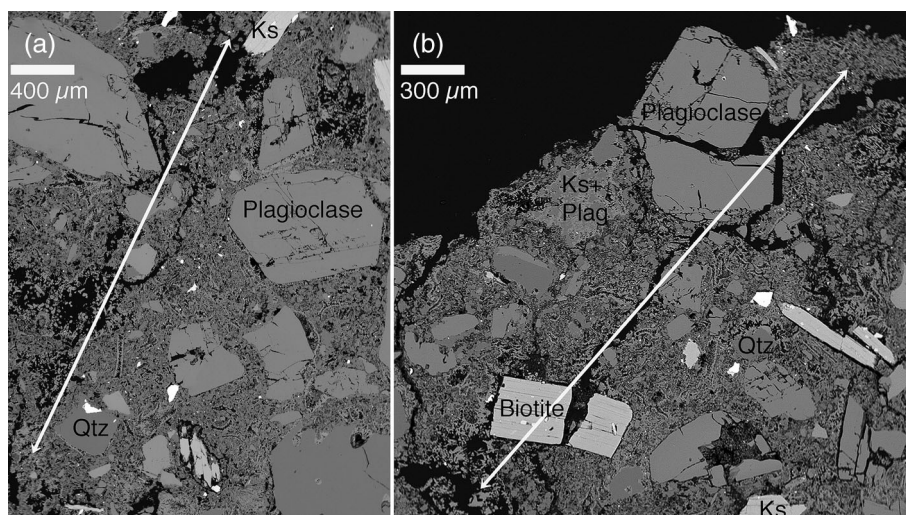

FIGURE 7 Enhanced dissolution in ignimbrite joints, revealed by BSE images from Figure 4a (corresponding with this image a—Martinez Canyon) and Figure 4b (corresponding with this image b—Weaver's Needle). Double arrows indicate the orientation of the joint. However, the joint width itself is much larger than the frame of the imagery. The phenocryst minerals were identified by EDS analyses, where Ks is orthoclase, plag is plagioclase and Qtz is quartz. The matrix between the phenocrysts is a mixture of glass and crystals. Pores appear black.

glass matrix itself. The least stable minerals appear to be smaller crystals of orthoclase (Ks in Figure 7) and biotite.

Dissolution appears to be taking place even inside the biotite (Figure 9a,c), but iron oxidation and reprecipitation also appears to be involved in altering biotite. Dissolved iron reprecipitates along the internal fractures and external surfaces. For example, the small D in Figure 9b shows a zone of brighter white (higher atomic number) material that corresponds with a stronger iron peak in the EDS in Figure 9d.

3.2 | Where fairy chimneys do not separate from a cliff face

Figure 5a shows a setting where the processes involved in the decay of ignimbrite columnar joints do not produce distinct separate fairy chimneys. From the appearance of Figure 5a, it is clear that enhanced decay does occur along joints, leading to distinct creases that could be sampled. However, mass wasting by rock fall and topple occurs before fairy chimneys separate from the main rock mass. Figure 10 provides possible insight for the lack of chimney separation. All of the subsamples collected from the arrow in Figure 5a were dominated by carbonate-rich precipitates inside fractures. In contrast, dissolution dominated in the other fractures (e.g., Figures 7 and 8), perhaps limiting carbonate build up. Dissolution of minerals and glass matrix does occur at the Figure 5a site but nowhere near as much as carbonate-rich precipitation. The host mineral in Figure 10 is quartz. Note that the EDS of the precipitate in Figure 10 is not only CaCO$_3$ but also has a strong sulphur peak suggestive of also gypsum (CaSO$_4$) along with minor elements Na, Mg, Al, Si and Fe.
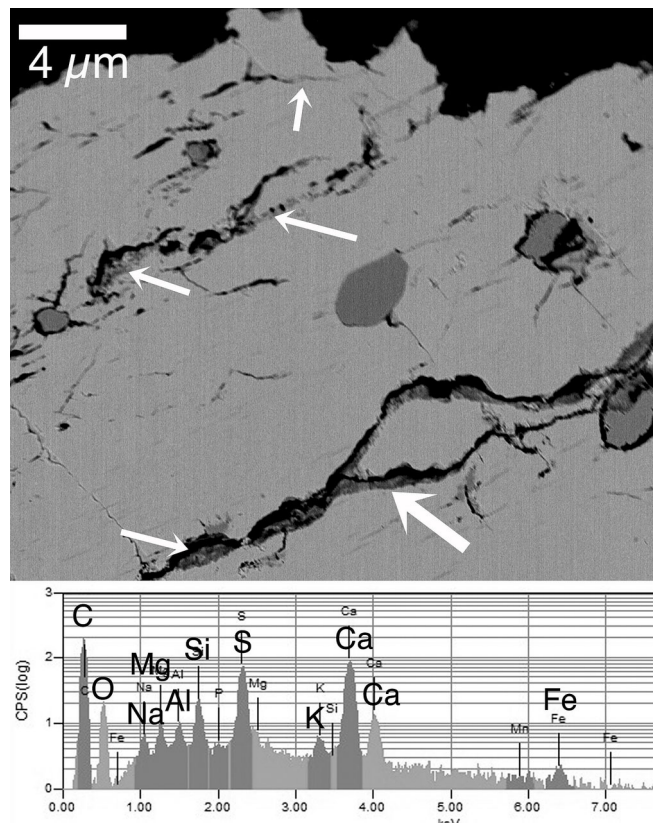

FIGURE 10 Carbonate wedging is a dominant process in the joints in Figure 4a. The BSE image and corresponding EDS analysis is consistent with carbonate (and perhaps gypsum) precipitated in fractures. The host mineral is quartz. The EDS analysis was collected at the largest white arrow. However, this EDS analysis is typical of the precipitates in the other fractures.
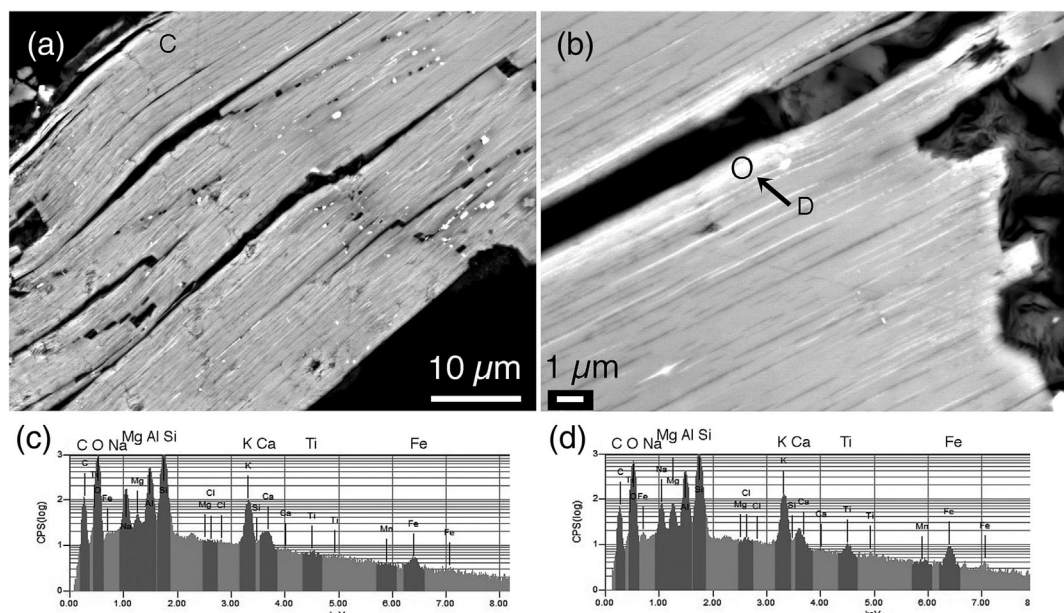

FIGURE 9 BSE imagery highlights biotite alteration in the Martinez Canyon joint (image a here from Figure 4a) and Weaver's Needle joint (image b here from Figure 4b). Alteration processes include enhanced dissolution in image (a) (the tiny black holes) and iron oxidation and reprecipitation in image (b). EDS analysis shown in image (c) was collected at the black 'C' in image (a) and indicates the composition of the biotite. EDS analysis shown in image (d) is a spot on the bright area in image (b) indicated by the open circle (see arrow in image b).

3.3 | Dissolution at a basal notch

An average and standard deviation of 10 paired samples from the notches around Figure 5b yielded a fourfold higher porosity of 27.30 ± 6.07% compared with a metre above the notch with a porosity of 5.47 ± 2.43%. This difference is statistically significant at $p < 0.001$. In the second notch investigation of 11 fairy chimneys experiencing ballistic impacts at the Fremont Saddle (see next Section 3.4), the 11 notches on 11 separate fairy chimneys experienced a threefold higher porosity of 29.93 ± 4.98% compared with a metre above each of the notches of 10.51 ± 2.25%. This difference is statistically significant at $p < 0.001$.

To better understand these differences, Figure 11a–d shows the connection between enhanced dissolution and observed flaking of the ignimbrite at the notch specifically in Figure 5b. Dissolution of the glass matrix dominates in Figure 11a,c,d, leading to detachment of both the matrix and phenocrysts. Note that these are cross-sections, so that even though a particle looks like it has already detached, it was embalmed in epoxy in the field and was still connected by a thread of rock material in the third dimension. Figure 11b shows the notch at a higher resolution where dissolution of both glass and minerals have a 'Swiss cheese' appearance from the ∼35% porosity. The interpretation made here is that porosity builds up to a threshold where a flake of ignimbrite detaches. The assumption made here is that the threshold for enhanced flaking is the porosity observed along the very surface of a notch (Figure 5b) or ∼25% to 30%.

3.4 | Mechanical impact associated with mass wasting

Figure 5c captures a topple stopped in mid-tilt by an adjacent fairy chimney. An examination of the surface around the contact point indicates that the toppling chimney bounced and slid before it came to a stop. Figure 12 shows one of the places where minerals shattered in response to this mechanical impact. The main slide groove was much larger in size, but difficult to sample; in contrast, the sample collected for Figure 12 was acquired by detaching a surface that had obviously been a point of contact. As noted in the methods section, the epoxy encasing the original sample was polished down a few tens of microns to highlight the internal shattering to impacted minerals.
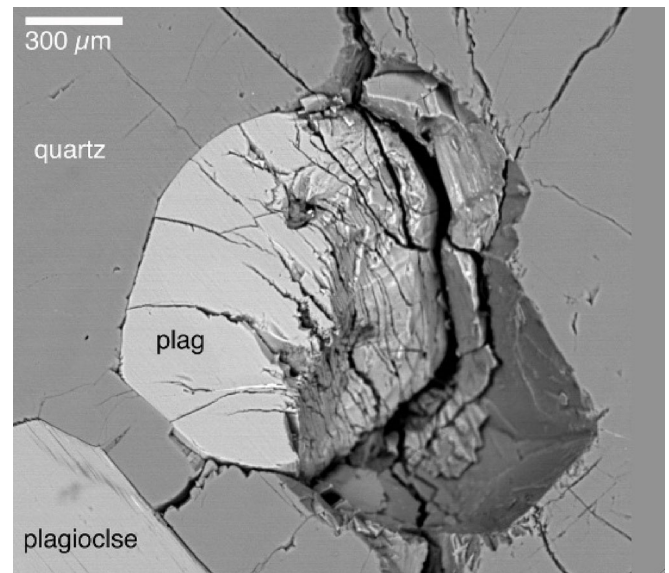

FIGURE 12 A toppling event of an ignimbrite chimney against an adjacent chimney resulted in mechanical shattering of plagioclase (plag) and quartz minerals, in a fashion roughly similar to bullet impacts in building stone (e.g., Campbell et al., 2022; Mol & Gomez-Heras, 2018).
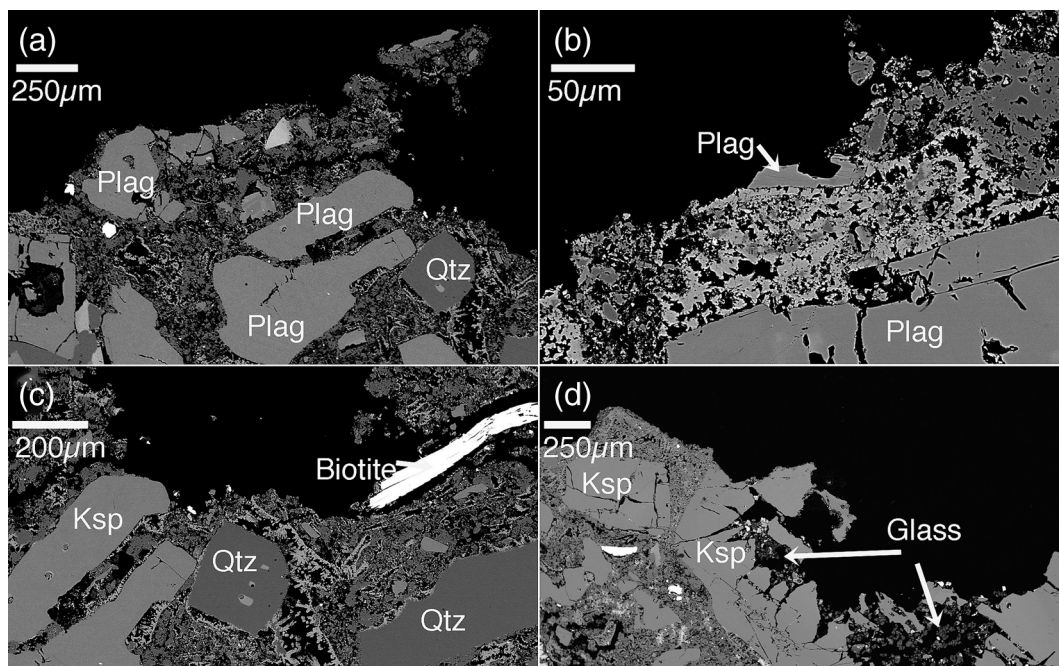

FIGURE 11 BSE images (a) through (d) typify how flaking occurs at the submillimetre scale at a notch at the base of a fairy chimney. Notches along the base of fairy chimneys typically occur at or just above the soil line, and the BSE images (a)–(d) came from samples collected at the white arrow in Figure 4a. The glass matrix dissolves to the point where it no longer holds the plagioclase (plag), orthoclase (Ksp), quartz (Qtz) and biotite in place. Epoxy applied to samples prior to removal helped preserve the very delicate surfaces undergoing detachment.

FIGURE 13 Investigation of ballistic impacts against fairy chimneys at Fremont Pass, Sonoran Desert. (a) Of the 100 fairy chimneys studied for the impact of rock falls, rock slides and topples against adjacent chimneys, 11 experienced impacts. Images (b)–(e) provide example with impact locations identified by arrows. Back-scattered electron microscope images (B)–(E) were from samples collected from the impact locations identified in corresponding images (b)–(e).
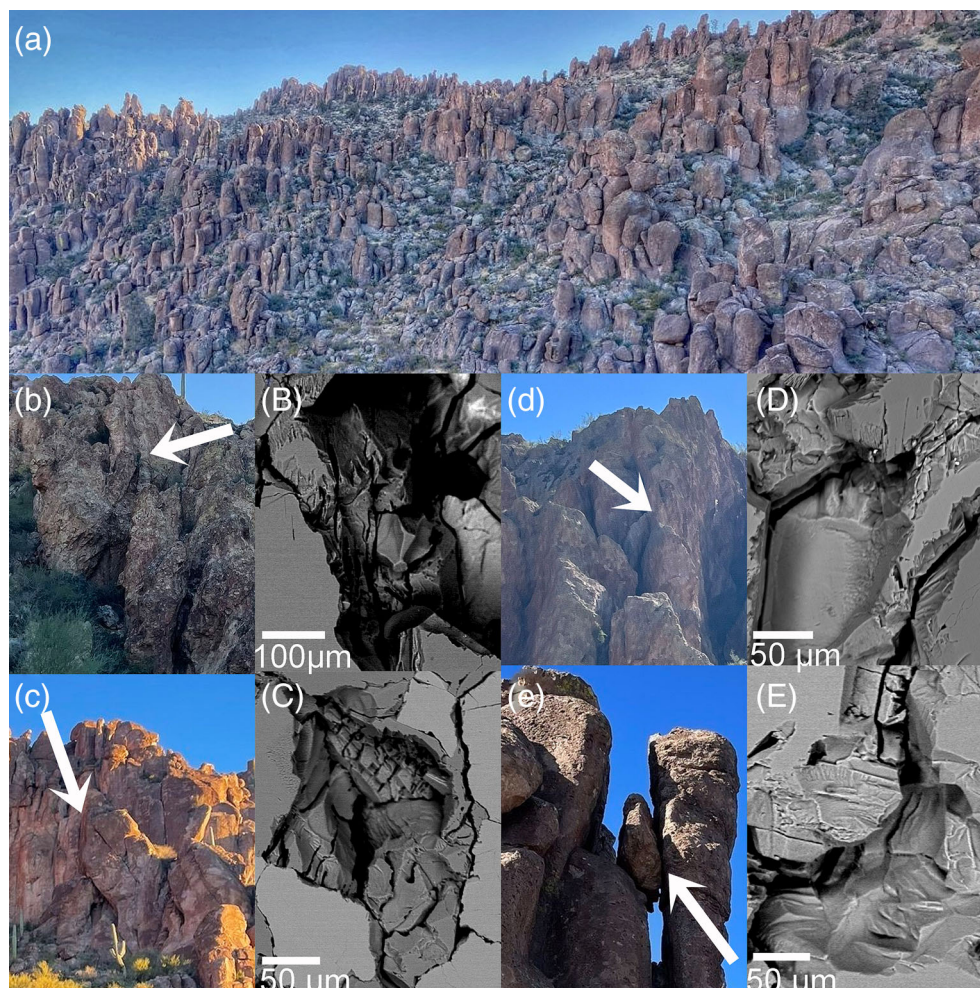
After observing Figure 12, a reviewer asked about the frequency and the size of these ballistic impacts caused by mass wasting. In response, an investigation revealed that 11 of the 100 fairy chimneys examined at Fremont Saddle area (Figure 13a) had current contact with mass wasted fairy chimneys as exemplified by Figure 13b–e where samples for SEM study yielded micrographs Figure 13B–E. VML dating does not work well in this context, because pulverized surfaces are not stable enough for varnish to form, and the length of time needed to erode the pulverized surface is not known. In some cases, areas of contact could not be measured directly to the inability of the author to reach the contact location; hence contact areas could only be estimated for seven impacted chimneys. An estimate of the size of the longest dimension of all of contact areas ranged from 5 cm to 1.4 m with areas of contact ranging from 15 cm^2 to 1.2 m^2.

3.5 | Case hardening

Inorganic materials and organisms both case harden the outer shell (weathering rind) of ignimbrite in the study area. Figure 2CH provides an example of where black fungi both decayed of the underlying rock and also stabilized decayed material; then, once the fungal 'dam' spalled off, the loose decayed particles trapped by the fungi eroded (Figure 2S).

Case-hardened surfaces of fairy chimneys sampled from Figure 5c,d display more complicated examples of case hardening. The case-hardened surface in Figure 5c is mostly inorganic (Figures 14a and 15a). Case hardening sampled at Figure 5d is mostly organic (Figure 14b) and includes inorganic constituents (Figure 15c,d). While Figure 14 images come from the outer 0.1 mm of the case-hardened weathering rind, the imagery in Figure 15 come from deeper into case-hardened weathering rind.

3.6 | Lichens and black fungi

Lichens and fungi growing on the surfaces of fairy chimneys can case harden (Figures 2CH and 14B) by holding in their structure the decayed remnants of a weathering rind. Lichens and also black fungi (Gadd, 2017; Leo et al., 2022), which are an ecological group of melanized fungi that specialize in extreme environments, also enhance rock decay within the weathering rind (Figure 16). Fungal hyphae, for example, are able to penetrate into the glass matrix and more resistant material like quartz (Figure 16a). Hyphae associated with lichens growing on the surface also penetrate into the weathering rind, fracturing even quartz (Figure 16b).

Although of images in Figure 16a,b were from samples collected from Figure 5d, Figure 16c,d illustrate that black fungi occur widely on the more mesic (e.g., north facing) microenvironments on fairy chimneys in the region. It is not possible to know for sure whether (i) hyphae followed pre-existing fractures, (ii) enlarged smaller pre-existing fractures, (iii) produced new fractures or (iv) once existed in a fracture in the past but died off. However, the jagged appearance of
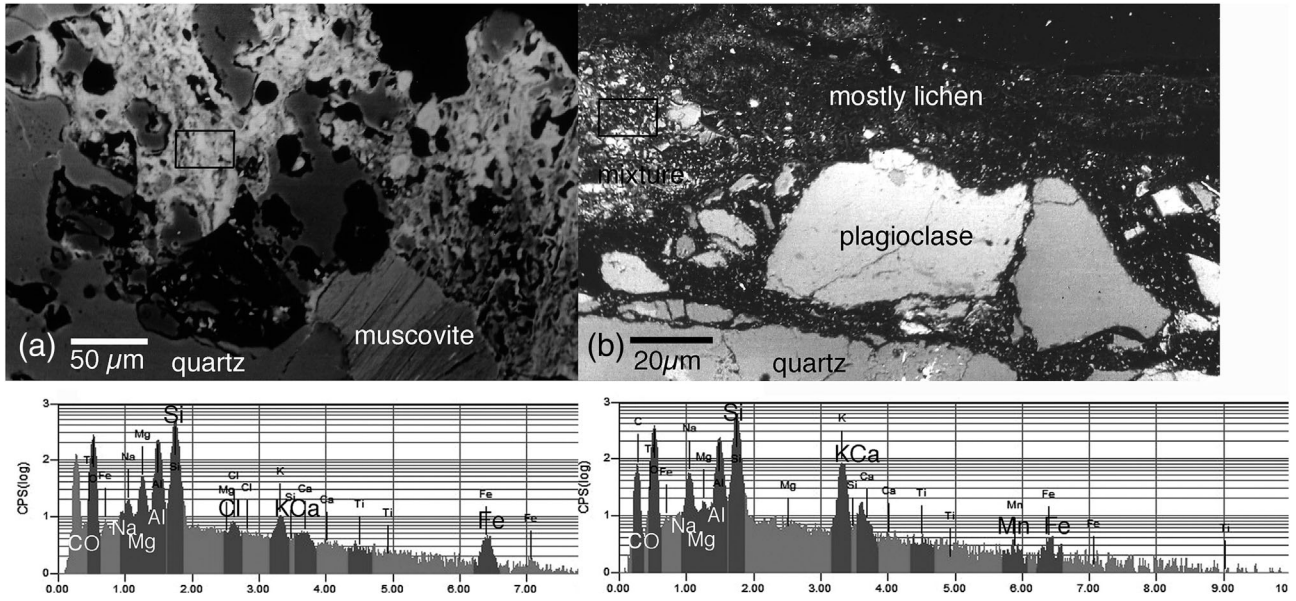
FIGURE 14 Case hardening develops when pores in the weathering rind are filled with material more resistant to erosion, aided also by the development of surface rock coatings. In image (a) (collected from the location in Figure 5c), the constituents are similar to the iron film that coats the surface—containing a mixture of clays (Si–Al–Mg–Na–Ka–Ca peaks) and iron oxyhydroxides. The box in image (a) is where the underlying EDS was acquired. In image (b), the case hardening (collected from the location in Figure 5d) is due to a mixture of lichen and partially dissolved rock varnish (Mn–Fe from the varnish; Mg–Al–Si–Ca from the clays). Small broken up pieces of orthoclase generated the strong K peak. The cause of the high Na is not known.
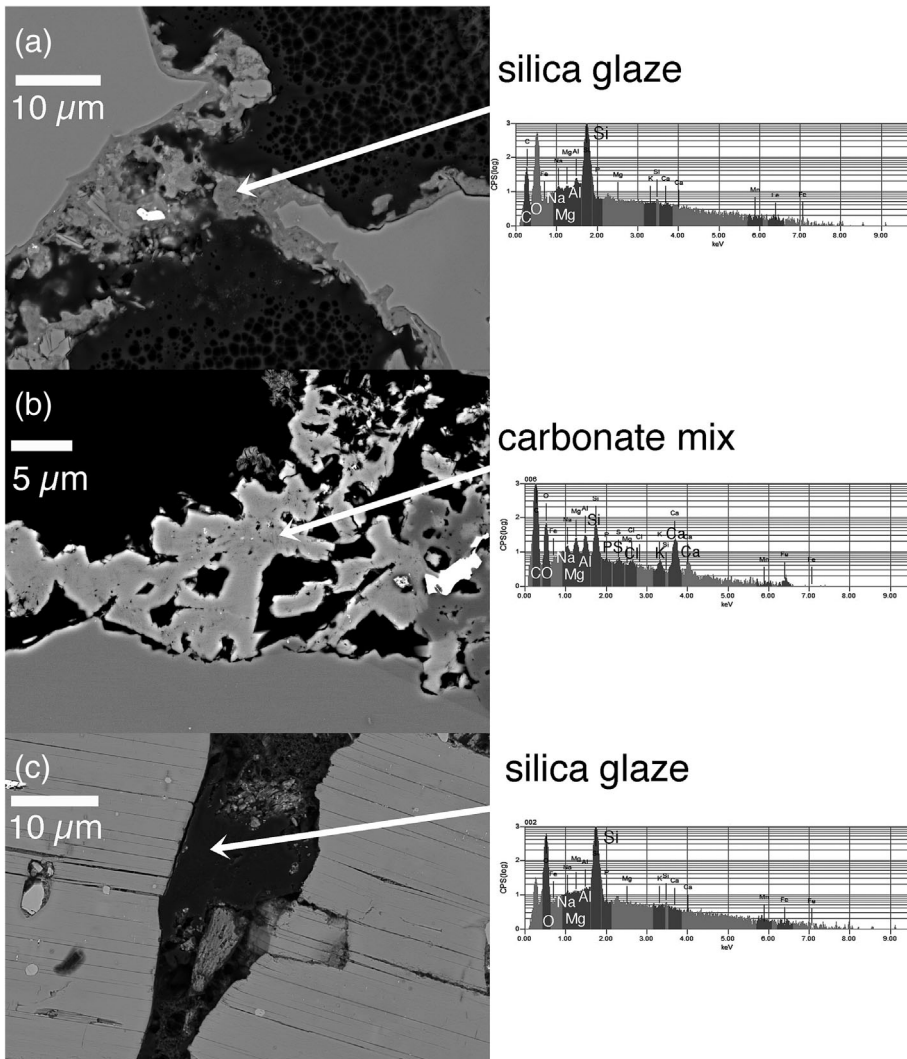

FIGURE 15 Case hardening surfaces of studied ignimbrite fairy chimneys results from different constituents infilling the pores of weathering rinds. The BSE/EDS images here provide examples. (a) Silica glaze infilling pores collected at Figure 5c deeper into the case-hardened shell (0.4 mm below the surface) than Figure 15a. (b) Carbonate with clays and minor elements 0.5 mm below the surface of Figure 5d. (c) Silica glaze infills a biotite fracture collected at Figure 5d. This image was acquired further inside (0.4 mm beneath the surface) the weathering rind than Figure 15b.
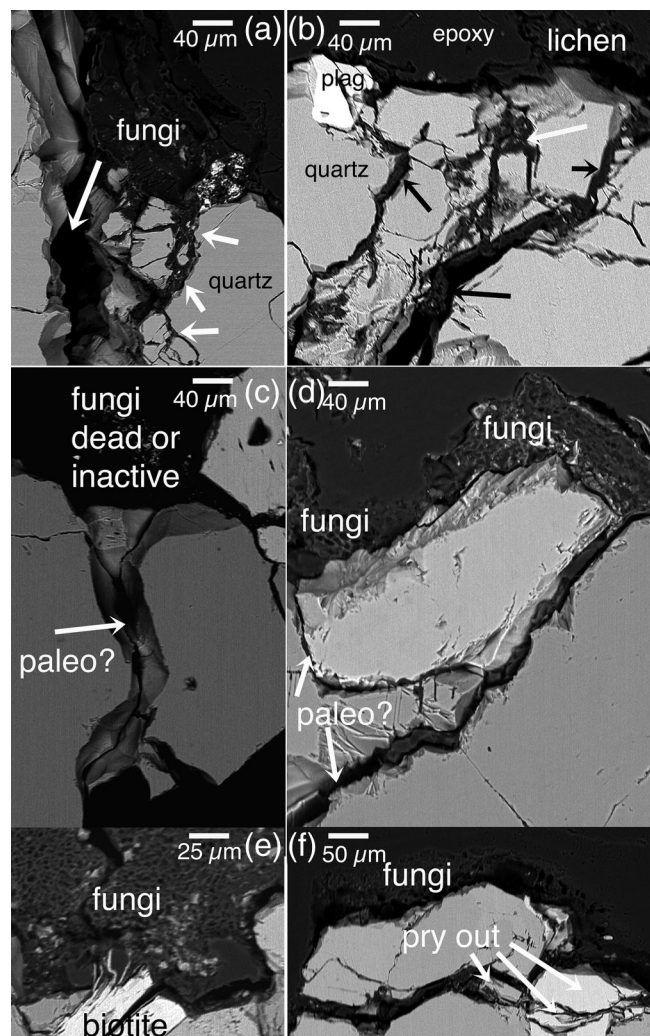
FIGURE 16 Black fungi (image a) and lichen (image b) occur on the northeast-facing side of the fairy chimney in Figure 5d. Images (c)–(f) came from the study of 10 north-facing chimney at Freemont Saddle (Figure 13a). Images (c) and (d) illustrate fracture that have inactive and active hyphae at the surface but with no hyphae in a fracture that perhaps might have once been widened by a palaeo-fungi hyphae. Image (e) illustrates black fungi that extended no hyphae and instead appears to be extracting bits and pieces of a decaying biotite. Image (f) illustrates fungal hyphae that has gotten under mineral fragments and appears to be 'prying' them from the chimney.

the quartz fracturing seen in Figure 16a–c is similar to the mechanical impact process seen in Figure 12 and carbonate wedging (a mechanical weathering process) observed in Figure 10.

Of the 10 chimneys sampled from Freemont Pass (Figure 13a) at 1 m above the surrounding soil surface on north-facing sides to investigate the impact of fungi and lichen hyphae, all ten 1000-μm-long electron microscope cross-section transects contained both fungi and lichen growing on surfaces. All transects had examples of both lichens and black fungi extending hyphae into fractures. Considering all electron microscope transects, the number of lichens with penetrating hyphae ranged from 3 to 9 and the number of black fungi with hyphae penetrating into the subsurface ranged from 12 to 28. The average and standard deviation of the length of all of the lichen and black fungi hyphae penetrating all 10 chimneys was 45 ± 39 and 37 ± 29 μm, respectively. The difference in penetration of lichens versus back fungi was not statistically significant. The fractures into which the lichen and black fungi were penetrating were longer with average and standard deviations of 133 ± 110 and 160 ± 135 μm, respectively.

3.7 | Rates of fairy chimney surface detachment

VML dating of the rock varnish that formed on 10 randomly selected fairy chimneys in Figure 6 reveals that almost all of the side and top surfaces last experienced surface flaking during the Holocene. It is important to note that these varnishes also formed on top of rock weathering rinds that all had some case hardening, most typically from combinations of silica glaze and reprecipitated rock varnish constituents. Chimney side samples came from a height of 1.5 m above the base of the chimney, avoiding lichens and fungi that destroy VML microlaminations. Top sampling occurred close to the centre of chimney tops. Figure 17 shows representative VML ultrathin sections from this study that range in age from late (Figure 17a) to early (Figure 17b) Holocene.

Of the 10 randomly selected fairy chimneys in Figure 6, and keeping in mind that the VML method can only provide minimum-limiting ages for when the rock surface last eroded, chimney sides experienced detachment much more recently than chimney tops (Table 1). Five of the chimneys experienced side erosion in the last millennia, and three more experienced surface loss in the late Holocene; only two chimneys had sides that eroded in the early Holocene. This contrasts with the tops of these same chimneys, where only one experienced erosion in the last millennia; seven last eroded in the early Holocene; and two last eroded at the Pleistocene/Holocene transition.

4 | DISCUSSION

4.1 | Comparison with prior fairy chimney research in Arizona

Hall and colleagues (Hall, 1993, 1996, 1998; Pallister et al., 1997) conducted a detailed study of tall, slender columns of ignimbrite in Arizona, focusing entirely on the fairy chimneys in Chiricahua National Monument. One key finding was that the basic form is set by columnar jointing in ignimbrites, a conclusion consistent with observations made in this study. A second key finding is that these joint planes provide avenues for water penetration and subsequent chemical decay (Wohletz, 2006), a conclusion consistent with the results here (Figures 7–10). A third key finding involves a set of assumptions to estimate the average erosion rate of 0.017 mm/year for the area of fairy chimneys (Hall, 1998). Such a long-term erosion rate would be consistent with the VML observations made here (Figure 17; Table 1). A fourth key finding is that a geological engineering analysis of column strength indicated the tuff itself is strong enough to not collapse under its own weight and hence not susceptible to collapse (Hall, 1996; Pallister et al., 1997); throughout this study, I noted that talus was uncommon along the base of fairy chimneys (Figures 2d, 4–6 and 13a), and where it did occur, it consisted mostly small blocks like those in Figure 5a,c; this is consistent with the overall mechanical stability of the many types of ignimbrites in Chiricahua National Monument
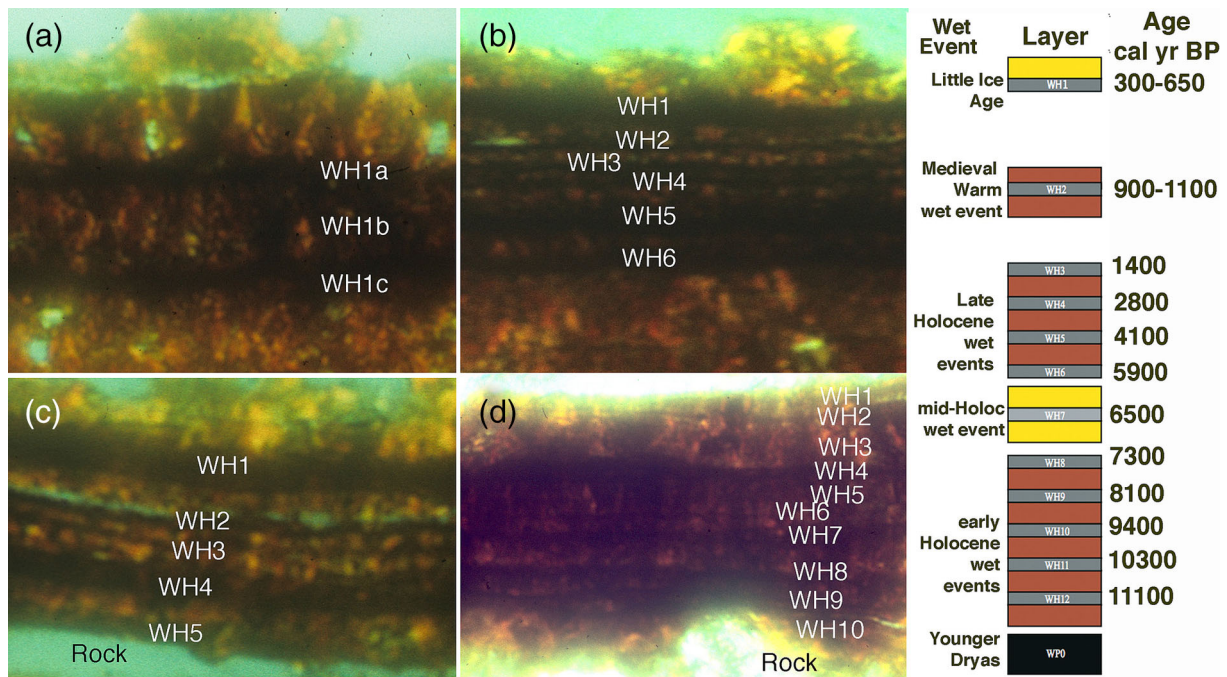
FIGURE 17 Examples of varnish microlamination ultrathin sections from samples collected from Figure 6. The annotations are nomenclature adopted from Liu & Broecker's (2007) Holocene calibration. WH means wet Holocene event that are the black laminations. The yellowish colour in the calibration reflects particularly arid conditions with the orange colour being slightly less arid intervals. Thickness of the varnish (30–60 μm for these sections) is not a function of age, but rather a product of the rate of varnish accumulation where more mesic locations accumulate varnish faster. Image (a), for example, is the same thickness as image (c) (30 μm), but formed fast enough to record the sublaminations of the Little Ice Age (WH1a, WH1b and WH1c in image a). Minimum ages are determined by the layer that formed first (at the bottom). Thus, the section of image (a) has a basal layer that is orange, forming between 900 and 650 cal year BP (between WH1 and WH2). The varnish in image (b) started forming before 6500 but after 7300 cal year BP. The varnish in image (c) started forming about 4100 cal year BP. The varnish in image (d) started forming between 10 300 and 9400 cal year BP, and the underlying surface was exposed by erosion before the varnish started to form. This is why VML provides minimum ages of the underlying erosion event. The calibration graphic shown on the right is based on Liu & Broecker (2007).

(Hall, 1993, 1996, 1998; Pallister et al., 1997) and also in this Superstition-Goldfield (Dombroski & Fodor, 2019) study area (Figure 3).

4.2 | Comparison with Cappadocia fairy chimneys

Terrestrial laser scanning and close-range photogrammetry revealed that the sides of Cappadocia chimneys erode by flaking patches that range in size from millimetres to centimetres (Yakar & Yilmaz, 2011; Yilmaz et al., 2009). The cause of this flaking was not evaluated in Cappadocia with electron microscopy—as done in this study (e.g., Figure 11). However, flakes of ignimbrite in the same size range as Cappadocia are ubiquitous throughout the entire study area (Figure 13).

Fairy chimneys of Cappadocia erode by toppling (Sari, 2021) and rock falls (Sari, 2022; Yakar & Yilmaz, 2011), processes that also occur in this study. Eleven of the 100 chimneys evaluated for ballistic impacts from mass wasting (Figure 13) experienced impacts from mass wasting events from adjacent chimneys. Still, the emphasis on toppling and rock falls in Cappadocia could mean that that these events are truly more common; if so, the reason such a difference could be due to the lower rock strength of the Cappadocia ignimbrite (Aydan et al., 2022; Kahraman, 2022) compared with the studied Arizona ignimbrites (Dombroski & Fodor, 2019; Hall, 1993).

Water penetration into capillaries in the Cappadocia tuff (Dincer & Bostanci, 2019) promotes dissolution via hydrolysis of the volcanic glass and feldspars (Garvia-Valles et al., 2003), the same process observed in BSE imagery (Figures 7–9 and 11). A small study into the role of fungi and lichen to promote water penetration into 10 chimneys at Figure 13a revealed that both lichen and fungi hyphae penetrate tens of micrometres into the north-facing aspects of chimneys, and this could also promote water penetration.

Through a study of mostly light microscopy of thin sections, Cappadocia lichens enhance mineral decay through hydrolysis and reduce the amount of water penetration into the tuffs, offering a strong protective effect (Garvia-Valles et al., 2003). This perspective was confirmed by more detailed observations at Üzümlu Church indicating high penetration of fungal hyphae of the lichens results in both enhanced decay and a protective effect (Municchia et al., 2018). As in Cappadocia, both decay and protective effects of lichens and fungi were also observed in this study (Figures 2CH and 16).

Case hardening at Cappadocia occurs through the formation of crusts that include both organic and inorganic constituents (Kazanci et al., 2022), as well as intentional heating to harden wall surfaces in early Medieval time (Kazanci et al., 2022). Case hardening similarly occurs through the addition of organic and inorganic materials to the outer surface of studied Arizona fairy chimneys (Figures 2CH, 14 and 15).

In situ cosmogenic ^{36}Cl analyses (Sarikaya et al., 2015) reveal that as long as the durable Cappadocia ignimbrite caps a chimney, erosion rates vary between 3.2 and 3.4 cm/ka. But after the caprock erodes away, rates of erosion increase an order of magnitude to ~28 cm/ka. The VML findings reported here do not yield the same units of

TABLE 1 VML minimum ages for the time when a surface last eroded.

Fairy chimney	VML age[a] (ka) chimney top	VML age[a] (ka) chimney side
1a	4.1	0.65–0.9
1b	2.8–4.1	0.3–0.65
1c	2.8–4.1	0.65–0.9
2a	9.4	7.3–8.1
2b	9.4	6.5–7.3
2c	8.1–9.4	6.5
3a	5.9	2.8
3b	5.9–6.5	4.1
3c	5.9–6.5	4.1
4a	9.4–10.3	0.65–0.9
4b	10.3	0.65
4c	9.4	0.65–0.9
5a	6.5–7.3	4.1
5b	6.5–7.3	4.1
5c	7.3–8.1	2.8–4.1
6a	12.5	0.65–0.9
6b	12.5	0.65–0.9
6c	12.5	4.1
7a	8.1	4.1
7b	8.1–9.4	2.5–4.1
7c	8.1	2.5–4.1
8a	2.8	0.65–0.9
8b	2.8	0.65–0.9
8c	2.8–4.1	0.65
9a	4.1–5.9	0.65–0.9
9b	4.1–5.9	0.65–0.9
9c	4.1	4.1
10a	9.4	8.1
10b	9.4	5.9
10c	10.3	4.1–5.9

Note: Numbers correspond with the fairy chimney identified in Figure 6. Fairy chimney letters a, b and c (e.g., 1a) denote the three separate samples with a VML sequence suitable for analysis.
[a]VML ages in thousands of calendar years before present (ka). The VML age is best interpreted as a minimum-limiting age for the last time that surface experienced erosion.

measurement of cm/ka for erosion but instead record when erosion last took place; however, the range of VML ages seen at Figure 6 (Figure 17; Table 1) would require erosion rates an order of magnitude lower in the studied fairy chimneys in Arizona. This is based on comparisons of VML and cosmogenic ^{10}Be ages in other studies in Arizona (Seong, Dorn, & Yu, 2016; Seong, Larson, et al., 2016).

4.3 | Rock decay's involvement in fairy chimney development: Towards a conceptual understanding

Rock decay plays a key role in fairy chimney development in Arizona's BRP, but only after ignimbrite deposition (Best et al., 2013), columnar joint formation (Pallister et al., 1997) and sufficient development of drainages to expose cliff faces. This section's purpose rests in moving towards a conceptual understanding on how rock decay processes interact at different timescales.

Rock decay's role starts with dissolution weakening columnar joints to the point at which the decayed material erodes away (Figures 7–9), effectively separating the fairy chimney from the main rock face (Figure 4). The rate at which joint dissolution takes place, unfortunately, is unknown.

Another knowledge gap in rock decay is why some columns do not separate from the rock face. Figure 10 reveals one possible explanation for the lack of chimney separation seen in Figure 5a. All of the subsamples collected from the arrow in Figure 5a were dominated by carbonate-rich precipitates inside fractures, in contrast to the other fractures where dissolution so dominated that carbonate has not built up. Dissolution of minerals and glass matrix does occur but nowhere near as much as carbonate-rich precipitation. Thus, the speculative hypothesis is that the balance between dissolution and carbonate accumulation is a factor in chimney separation. Carbonate precipitation is known to widen nanoscale fractures in the Sonoran Desert, part of the general physical weathering process known as 'dirt cracking' where strontium isotope analyses reveal the carbonate derives from dust storms (Dorn, 2011). The host mineral in Figure 10 is quartz. Note that the EDS of the precipitate in Figure 10 is not only $CaCO_3$ but also has a strong sulphur peak suggestive of also gypsum ($CaSO_4$) along with minor elements Na, Mg, Al, Si and Fe. In summary, column separation occurs where dissolution is the dominant process in joints, but dirt cracking may interfere with fairy chimney separation.

Rock decay around the bases of studied fairy chimneys, at notches (e.g., Figure 5b), occurs from dissolution rates 4× faster than the interior of a column. Notch development undermines fairy chimneys, leading to mass wasting events (e.g., Figures 5 and 13). At one field site, 11% of the studied fairy chimneys experienced the impact of wasted material (Figures 12 and 13). Other studies have noted that notch forms commonly develop near the base of many different types of desert rocks (Mabbutt, 1977; Meek & Dorn, 2000; Oberlander, 1972; Shtober-Zisu et al., 2017; Twidale, 1990; Twidale & Campbell, 1992). This study specifically links the microscopic processes of dissolution leads to enhanced porosity of 25% to 30% (Figure 11) that in turn generates a notch at the base of a fairy chimney (Figure 5b). The rate of erosion at a notch must be faster than the rate of rock varnish formation, because the flake scars in most of the notches lack rock varnish; this indicates that the last flaking event was younger than the <350 years it takes to develop a noticeable varnish in this region (e.g., Dorn, 2014).

VMLs (Figure 17) provide a method to understand the stability (or lack thereof) of desert surfaces. These VML only accumulate when there is no erosion—not even at the nanometre scale, and their layering pattern records for how long the varnish has accumulated (Table 1). A study of randomly selected fairy chimneys (Figure 6) revealed that the sides of the chimneys are much less stable than the tops, in all 10 sampled chimneys (Table 1). An obvious explanation is that the near-vertical slopes of fairy chimney sides promote detachment. In other words, once the porosity of the weathering rind under the varnish reaches a threshold of ~25% to 30%, a vertical face provides no lateral support to slow detachment. It is also possible that a chimney top receives even less contact with moisture; a concept in geomorphic research is that contact-time with water is a key factor

in decaying rock material (Oberlander, 1974; Ruxton, 1958; Twidale, 1974, 2002; Twidale & Mueller, 1988; Wahrhaftig, 1965); water running off the tops of the chimneys might result in less time in contact with water. Regardless of this speculation on the reason for more stable tops and sides, VML data provide a general understanding of the timescale of the rates of fairy chimney flaking in the study region.

Rock decay also modifies the surfaces of studied fairy chimneys through the actions of lichens and black fungi (Figure 14). All 10 fairy chimneys sampled on north-facing aspects from Freemont Pass (Figure 13a) hosted both lichens and black fungi with hyphae penetrating into fractures. The average and standard deviation of the length of all of the lichen and black fungi hyphae on the 10 chimneys was 45 ± 39 and 37 ± 29 μm, respectively. The fractures themselves were much longer with average and standard deviations of 133 ± 110 and 160 ± 135 μm, respectively. Black fungi (Gadd, 2007, 2017) and lichen (Brady et al., 1999; Seaward, 1988) in other research also fracture the underlying rock by sending hyphae into fractures and perhaps widening them. In contradistinction, lichen can also have a protective effect through case hardening surfaces (Figure 13), and this is also true in the broader literature for both black fungi (Gadd, 2017; Viles & Goudie, 2004) and lichen (Jones & WIlson, 1986; Mottershead & Lucas, 2000; Viles & Goudie, 2004).

The most rapid rock-decay process studied here involves ballistic impacts on adjacent chimneys from mass wasting. The next fastest process is likely notch development and surface erosion, based on the lack of rock varnish that typically takes <350 years be noticeable in the field. VML data from one field area indicates that flaking of fairy chimney sides and tops occurs at time scales an order of magnitude (or more) longer than notch erosion. I speculate that joint dissolution occurs at even longer timescales. Unfortunately, the timescale of lithobiont-generated rock decay is unknown.

Some of the other microscopic processes observed here in electron micrographs have been reported in studies of rock decay in other settings. For example, biotite splitting by iron mobilization and reprecipitation (Figure 9) occurs in a variety of climatic settings (Dixon et al., 2002; Pope et al., 1995). The case hardening seen here involving infilling of weathering rind pores (Figures 14 and 15) similarly occurs widely in different environmental contests (Broxton et al., 2014; Conca, 1982; Dorn, 2004; Dorn et al., 2012, 2017; Viles & Goudie, 2004). Carbonate precipitation is known to widen nanoscale fractures (Dorn, 2011)—turning minerals and glass into silt-sized material. This carbonate wedging process is part of the dirt cracking physical rock-decay process (Dorn & Walker, 2022)—a process noted (Figure 10) at one location in this study (Figure 5a).

5 | CONCLUSION

Tall and narrow columns of ignimbrite form dramatic landscapes that are of such interest that they result in the creation of national parks like Göreme Valley in Turkey and Chiricahua National Monument in the United States. Increasingly known by the term 'fairy chimney' around the globe, their scientific study outside of Cappadocia, Turkey, has been limited in scope to a few investigations (at most) at any given site. Within the US state of Arizona, for example, with hundreds of square kilometres of exposed ignimbrite hosting an uncounted

number of fairy chimney sites certainly numbering in the hundreds, only Hall (1993, 1996, 1998) presented geomorphic scholarship on mass wasting processes generating this striking landform in Chiricahua National Monument.

This first research effort into the rock-decay processes involved in Arizona fairy chimney development highlights the potential for future research across the Basin and Range (Figures 1 and 3) of Arizona. Within the Goldfield-Superstition volcanic province of ignimbrite calderas and related ash-flow tuffs, (Dombroski & Fodor, 2019), I focus on two areas of fairy chimneys that are well known to outdoor enthusiasts (but not to geomorphologists): the Martinez Canyon area (33.1672, −111.1556) and the Weaver's Needle area (33.4331, −111.3704).

Electron microscopy of fairy chimneys in the Goldfield-Superstition volcanic province reveals a variety of different processes impacting fairy chimney. Dissolution of columnar joints plays a key role in chimney separation from a cliff face. Notches developed around the base of fairy chimney also result from mineral dissolution, leading to instability and mass wasting. Rock fall and toppling, while less common than in Cappadocia, Turkey, do occur and lead to ballistic impacts against adjacent chimneys and talus. Case hardening of fairy chimney surfaces develop when organic (e.g., lichens) and inorganic (e.g., iron films and silica glaze) materials infill pores in the weathering rinds of fairy chimneys. However, lichens as well as black fungi also increase decay of weathering rinds—especially on north-facing aspects.

The rock-decay processes of fairy chimney development studied in Arizona are similar to prior scholarship on fairy chimneys in Cappadocia and ignimbrite landforms in other regions. However, the fairy chimneys in the Goldfield-Superstition volcanic province, as well as those in Chiricahua National Monument (Hall, 1993, 1996, 1998), appear to experience rock decay-generated erosion at a pace an order of magnitude slower than at Cappadocia (Sarikaya et al., 2015).

CONFLICT OF INTEREST STATEMENT

No potential conflict of interest was reported by the author.

DATA AVAILABILITY STATEMENT

All available data are presented in the submission.

ORCID

Ronald I. Dorn 🆔 https://orcid.org/0000-0003-1343-4556

REFERENCES

Aguilera, E.Y., Hernando, I. & Rabassa, J. (2017) Landscapes developed on ignimbrites. In: *Advances in geomorphology and quaternary studies in Argentina*. Amsterdam: Springer, pp. 1–48. Available from: https://link.springer.com/chapter/10.1007/978-3-319-54371-0_1

Ahmad, M., Ansari, M.K., Sharma, L.K., Singh, R. & Singh, T. (2017) Correlation between strength and durability indices of rocks—soft computing approach. *Procedia Engineering*, 191, 458–466. Available from: https://doi.org/10.1016/j.proeng.2017.05.204

Anjbaran, R. (2018) Azarbaijan fairy chimneys [translation]. *GMPJ*, 7(1), 48–60.

Aydan, O., Kumsar, H. & Ulusay, R. (2022) The inference of physico-mechanical properties of tuffs of Cappadocia region and Phrygian Valley of Turkey from needle penetration index (NPI). In: Ohta, T., Ito, T. & Osada, M. (Eds.) *Rock mechanics and engineering geology in volcanic fields*. London: CRC Press, pp. 1–7. Available from: https://doi.org/10.1201/9781003293590-29

Best, M.G., Christiansen, E.H. & Gromme, S. (2013) Introduction: the 36-189 Ma southern Great Basin, USA, ignimbrite province and flareup: swarms of subduction-related supervolcanoes. *Geosphere*, 9(2), 260–274. Available from: https://doi.org/10.1130/GES00870.1

Bouzekraoui, H., Barakat, A., ElYoussi, F., Touhami, F., Mouaddine, A., Hafid, A. et al. (2018) Mapping geosites as gateways to the geotourism management in Central High-Atlas (Morocco). *Quaestiones Geographicae*, 37(1), 87–102. Available from: https://doi.org/10.2478/quageo-2018-0007

Brady, P.V., Dorn, R.I., Brazel, A.J., Clark, J., Moore, R.B. & Glidewell, T. (1999) Direct measurement of the combined effects of lichen, rainfall, and temperature on silicate weathering. *Geochimica et Cosmochimica Acta*, 63(19–20), 3293–3300. Available from: https://doi.org/10.1016/S0016-7037(99)00251-3

Broxton, D., Porter, D., Bass, A. & Domingue, R. (2014) Case hardening and the weather resistance of rhyolitic tuff: preservation of the cavates and petroglyphs of Bandelier National Monument. *International Masonry Conference 2014 in Guimarães*, 9, 1–16.

Campbell, O., Blenkinsop, T. & Mol, L. (2022) Bullet impacts in building stone excavate approximately conial craters, with dimensions that are controlled by target material. *Scientific Reports*, 12(1), 17634. Available from: https://doi.org/10.1038/s41598-022-22624-z

Campbell, E.M. & Twidale, C.R. (1991) The evolution of bornhardts in silicic volcanic rocks in the Gawler Ranges. *Australian Journal of Earth Sciences*, 38(1), 79–93. Available from: https://doi.org/10.1080/08120099108727957

Conca, J. (1982) Case hardening of the surface features: earth analogs to the Martian surface. *Lunar and Planetary Science*, 13, 125–126.

Deniz, B.E. & Topal, T. (2021) Durability assessment of some Cappadocian tuffs using factor analysis, multiple regression analysis, and analytical hierarchy process. *Bulletin of Engineering Geology and the Environment*, 81, 6. Available from: https://doi.org/10.1007/s10064-10021-02510-10060

Dincer, I. & Bostanci, M. (2019) Capillary water absorption characteristics of some Cappadocian ignimbrites and the role of capillarity on their deterioration. *Environment and Earth Science*, 78(1), 7. Available from: https://doi.org/10.1007/s12665-12018-17993-12662

Dixon, J.C., Thorn, C.E., Darmody, R.G. & Campbell, S.W. (2002) Weathering rinds and rock coatings from an Arctic alpine environment, northern Scandinavia. *Geological Society of America Bulletin*, 114(2), 226–238. Available from: https://doi.org/10.1130/0016-7606(2002)114<0226:WRARCF>2.0.CO;2

Dogan, U., Kocyiglt, A. & Yilmaz, E. (2019) Geomorphological evolutionary history of the Melendiz River Valley, Cappadocia, Turkey. *Mediterranean Geoscience Reviews*, 1, 203–222. Available from: https://doi.org/10.1007/s42990-42019-00012-42996

Dombroski, B.A. & Fodor, R.V. (2019) The Miocene Goldfield-Superstition volcanic province, Central Arizona, USA: geochemically distinct rhyolite sources, 20.5 to 19 Ma. *Lithos*, 330-331(April), 139–159. Available from: https://doi.org/10.1016/j.lithos.2019.1002.1008

Dorn, R.I. (1995) Digital processing of back-scatter electron imagery: a microscopic approach to quantifying chemical weathering. *Geological Society of America Bulletin*, 107(6), 725–741. Available from: https://doi.org/10.1130/0016-7606(1995)107<0725:DPOBSE>2.3.CO;2

Dorn, R.I. (2004) Case hardening. In: Goudie, A.S. (Ed.) *Encyclopedia of geomorphology*. London: Routledge, pp. 118–119.

Dorn, R.I. (2011) Revisiting dirt cracking as a physical weathering process in warm deserts. *Geomorphology*, 135(1-2), 129–142. Available from: https://doi.org/10.1016/j.geomorph.2011.08.010

Dorn, R.I. (2014) Chronology of rock falls and slides in a desert mountain range: case study from the Sonoran Desert in south-central Arizona. *Geomorphology*, 223, 81–89. Available from: https://doi.org/10.1016/j.geomorph.2014.07.005

Dorn, R.I. (2016) Identification of debris-flow hazards in warm deserts through analyzing past occurrences: case study in South Mountain, Sonoran Desert, USA. *Geomorphology*, 273, 269–279. Available from: https://doi.org/10.1016/j.geomorph.2016.08.013

Dorn, R.I. (2018) Necrogeomorphology and the life expectancy of desert bedrock landforms. *Progress in Physical Geography: Earth and Environment*, 42(5), 566–587. Available from: https://doi.org/10.1177/0309133318795839

Dorn, R.I. & Brady, P.V. (1995) Rock-based measurement of temperature-dependent plagioclase weathering. *Geochimica et Cosmochimica Acta*, 59(13), 2847–2852. Available from: https://doi.org/10.1016/0016-7037(95)00159-W

Dorn, R.I., Dorn, J., Harrison, E., Gutbrod, E., Gibson, S., Larson, P. et al. (2012) Case hardening vignettes from the western USA: convergence of form as a result of divergent hardening processes. *Association of Pacific Coast Geographers Yearbook*, 74(1), 1–12. Available from: https://doi.org/10.1353/pcg.2012.0003

Dorn, R.I., Mahaney, W.C. & Krinsley, D.H. (2017) Case hardening: turning weathering rinds into protective shells. *Elements*, 13(3), 155–158. Available from: https://doi.org/10.2113/gselements.13.3.165

Dorn, R.I. & Walker, I.J. (2022) Dirt cracking as a rock fracture-wedging process in the Mediterranean climate of Victoria, British Columbia, Canada. *Catena*, 210, 105920. Available from: https://doi.org/10.1016/j.catena.2021.105920

Duszyński, F., Ford, D.C., Goudie, A.S. & Migoń, P. (2021) Rock properties and rock-controlled landforms. *Geological Society, London, Memoirs*, 58(1), 151–171. Available from: https://doi.org/10.1144/M1158-2021-1141

Emre, O. & Guner, Y. (1988) ÜrgÜp yöresi peribacalarının morfojenezi. *Jeomorfoloji Dergisi*, 16, 23–30.

Enlows, H.E. (1955) Welded tuffs of Chiricahua National Monument, Arizona. *Geological Society of America Bulletin*, 66(10), 1215–1246. Available from: https://doi.org/10.1130/0016-7606%281955%2966%5B1215:WTOCNM%5D2.0.CO;2

Erguler, Z.A. (2009) Field-based experimental determination of the weathering rates of the Cappadocian tuffs. *Engineering Geology*, 105(3-4), 186–199. Available from: https://doi.org/10.1016/j.enggeo.2009.02.003

Ferguson, C.A. & Skotnicki, S.J. (1995) Geology of the Florence Junction and southern portion of the Weavers Needle 7.5′ quadrangles, Pinal County, Arizona. Arizona Geological Survey Open-File Report 95-10, pp. 1–27.

Gadd, G.M. (2007) Geomycology: biogeochemical transformations of rocks, minerals, metals and radionuclides by fungi, bioweathering and bioremediation. *Mycological Research*, 111(1), 3–49. Available from: https://doi.org/10.1016/j.mycres.2006.12.001

Gadd, G.M. (2017) Fungi, rocks, and minerals. *Elements*, 13(3), 171–176. Available from: https://doi.org/10.2113/gselements.13.3.171

Garvia-Valles, M., Topal, T. & Vendrell-Saz, M. (2003) Lichenic growth as a factor in the physical deterioration or protection of Cappadocian monuments. *Environmental Geology*, 43(7), 776–781. Available from: https://doi.org/10.1007/s00254-002-0692-y

Hall, D.B. (1993) *Geomorphology of welded tuffs, Chiricahua National Monument, southeastern Arizona*. Ph.D. Dissertation. Tucson: University of Arizona.

Hall, D.B. (1996) Modelling failure of natural rock columns. *Geomorphology*, 115(2), 123–134. Available from: https://doi.org/10.1016/0169-555X(95)00126-P

Hall, D.B. (1998) Using digital elevation models to calculate a time-averaged landscape denudation rate. *Physical Geography*, 19(4), 341–349. Available from: https://doi.org/10.1080/02723646.1998.10642655

Hall, K., Thorn, C.E. & Sumner, A. (2012) On the persistence of 'weathering'. *Geomorphology*, 149–150, 1–10. Available from: https://doi.org/10.1016/j.geomorph.2011.12.024

Hetényi, G., Taisne, B., Garel, F., Medard, E., Bosshard, S. & Mattsson, H.B. (2012) Scales of columnar jointing in igneous rocks: field measurements and controlling factors. *Bulletin of Volcanology*, 74(2), 457–

482. Available from: https://doi.org/10.1007/s00445-00011-00534-00444

Howard, K.A., John, B.E., Nielson, J.E., Miller, J.M.G. & Wooden, J.L. (2013) Geologic map of the Topock 7.5′ quadrangle, Arizona and California. U.S. Geological Survey Scientific Investigations Map and Pamphlet 3236. pp. 1–60.

Jeong, A., Cheung, S.Y., Walker, I.J. & Dorn, R.I. (2018) Urban geomorphology of an arid city: case study of Phoenix Arizona. In: Thornbush, M.J. & Allen, C.D. (Eds.) *Urban geomorphology: landforms and processes in cities*. Amsterdam: Elsevier. Available from: https://doi.org/10.1016/B978-0-12-811951-8.00010-2

Jessup, B.S., Hahm, W.J., Miller, S.N., Kirchner, J.W. & Riebe, C.S. (2011) Landscape response to tipping points in granite weathering: the case of stepped topography in the Southern Sierra Critical Zone Observatory. *Applied Geochemistry*, 26, 548–550. Available from: https://doi.org/10.1016/j.apgeochem.2011.03.026

Jones, D. & Wilson, M.J. (1986) Biomineralisation in crustose lichens. In: Leadbeater, B.S.C. & Riding, R. (Eds.) *Biomineralisation in lower plants and animals*. Oxford: Clarendon Press, pp. 91–105.

Kahraman, S. (2022) Estimating the physico-mechanical properties of pyroclastic rocks from electrical resistivity. *Pure and Applied Geophysics*, 179(1), 301–309. Available from: https://doi.org/10.1007/s00024-021-02898-6

Kaljahi, E.A. & Birami, F.A. (2015) Engineering geological properties of the pyroclastic cone-shaped rocky houses of Kandovan, Iran. *Bulletin of Engineering Geology and the Environment*, 74(3), 959–969. Available from: https://doi.org/10.1007/s10064-014-0679-4

Kazanci, N., Ozguneylioglu, A., Oncel, S.M., Erturac, M.K. & Sahiner, E. (2022) Crust occurrence on Galatin rock-cut dwelling in central Anatolia Turkey. *Geoarchaeology*, 37(4), 658–681. Available from: https://doi.org/10.1002/gea.21910

Klaer, W. (1993) Beobachtungen zu Formen der Verwitterung und Abtragung auf Sandsteinfelsen und Graniten in der algerischen Sahara. *Wirzburger Geographische Arbeiten*, 87, 121–132.

Kuzucuoglu, C. (2019) Geology and geomorphology of the Cappadocia Province, Turkey. *Mediterranean Geoscience Reviews*, 1(2), 163–166. Available from: https://doi.org/10.1007/s42990-019-00015-3

Larson, P.H., Dorn, R.I., Palmer, R.E., Bowles, Z., Harrison, E., Kelley, S., et al. (2014) Pediment response to drainage basin evolution in south-central Arizona. *Physical Geography*, 35(5), 369–389. Available from: https://doi.org/10.1080/02723646.2014.931089

Larson, P.H., Dorn, R.I., Skotnicki, S.J., Seong, Y.B., Jeong, A. & DePonty, J. (2020) Impact of drainage integration on basin geomorphology and landform evolution: a case study along the Salt and Verde rivers, Sonoran Desert, USA. *Geomorphology*, 369, 107439. Available from: https://doi.org/10.1016/j.geomorph.2020.107439

Leo, F.D., Marchetta, A. & Urzi, C. (2022) Black fungi on stone-built heritage: current knowledge and future outlook. *Applied Sciences*, 12(8), 3969.

Liu, T. & Broecker, W.S. (2007) Holocene rock varnish microstratigraphy and its chronometric application in drylands of western USA. *Geomorphology*, 84(1-2), 1–21. Available from: https://doi.org/10.1016/j.geomorph.2006.06.008

Liu, T. & Broecker, W.S. (2013) Millennial-scale varnish microlamination dating of late Pleistocene geomorphic features in the drylands of western USA. *Geomorphology*, 187, 38–60. Available from: https://doi.org/10.1016/j.geomorph.2012.12.034

Mabbutt, J.C. (1977) *Desert landforms*. Canberra: Australian National University Press.

McBride, E.F. & Picard, M.D. (2000) Origin and development of tafoni in Tunnel Spring Tuff, Crystal Peak, Utah, USA. *Earth Surface Processes and Landforms*, 25(8), 869–879. Available from: https://doi.org/10.1002/1096-9837(200008)25:8<869::AID-ESP104>3.0.CO;2-F

Meek, N. & Dorn, R.I. (2000) Is mushroom rock a ventifact? *California Geology*, (November/December), 18–20.

Mol, L. & Gomez-Heras, M. (2018) Bullet impacts and built heritage damage 1640-1939. *Heritage Science*, 6(1), 35. Available from: https://doi.org/10.1186/s40494-018-0200-7

Moon, V. (1993) Geotechncal characteristics of ignimbrite: a soft pyroclastic rock type. *Engineering Geology*, 35(1-2), 33–48. Available from: https://doi.org/10.1016/0013-7952(93)90068-N

Mottershead, D.N. & Lucas, G. (2000) The role of lichens in inhibiting erosion of a soluble rock. *The Lichenologist*, 32(6), 601–610. Available from: https://doi.org/10.1006/lich.2000.0300

Mueller, J.E. & Twidale, C.R. (1988) Landform development of City of Rocks State Park and Giant of the Mimbres. *New Mexico Geological Society Guidebook*, 39, 185–190.

Municchia, A.C., Bartoli, F., Taniguchi, Y. & Giordani, P. (2018) Evaluation of the biodeterioration activity of lichens in the Cave Church of ÜzÜmlÜ (Cappadocia, Turkey). *International Biodeterioration & Biodegradation*, 127, 160–169. Available from: https://doi.org/10.1016/j.ibiod.2017.1011.1023

Oberlander, T.M. (1972) Morphogenesis of granite boulder slopes in the Mojave Desert, California. *Journal of Geology*, 80(1), 1–20. Available from: https://doi.org/10.1086/627710

Oberlander, T.M. (1974) Landscape inheritance and the pediment problem in the Mojave Desert of Southern California. *American Journal of Science*, 274(8), 849–875. Available from: https://doi.org/10.2475/ajs.274.8.849

Oberlander, T.M. (1977) Origin of segmented cliffs in massive sandstones of southeastern Utah. In: Doehring, D.O. (Ed.) *Geomorphology in arid regions*, Proceedings Eighth Annual Geomorphology Symposium: Binghamton. New York: Routledge, pp. 79–114.

Oh, J.-S., Seong, J.B., Larson, P.H., Hong, S.-C. & Yu, B.Y. (2020) Asymmetric hillslope retreat revealed from talus flatirons on rock peak, San Tan Mountains, Arizona, United States: assessing caprock lithology control on landscape evolution. *Annals of the Association of American Geographers*, 110(1), 98–119. Available from: https://doi.org/10.1080/24694452.2019.1624421

Pallister, J.S., duBray, E.A. & Hall, D.B. (1997) Guide to the volcanic geology of Chiricahua National Monument and vicinity, Cochise County, Arizona. U.S. Geological Survey Miscellaneous Investigations Series Map I-2541. pp. 1–11.

Pasquare, G. (1968) Geology of the Cenozoic volcanic area of Central Anatolia. *Accademia, Nazionale Dei Lincei, Rome*, 9(8), 57–201.

Paterno, M.C.P. (1999) *A study of the weathering of volcanic tuffs in a tropical environment, including the evaluation of a consolidant*. M.S. Thesis. Philadelphia: University of Pennsylvania. Available from: https://repository.upenn.edu/hp_theses/291, pp. 1–137.

Pereira, L.S. (2019) The geoheritage o the Paraiba State South Coast, Brazil. *International Journal of Earth Science and Geology*, 1(1), 51–58. Available from: https://doi.org/10.18689/ijeg-1000106

Pope, G., Dorn, R.I. & Dixon, J. (1995) A new conceptual model for understanding geographical variations in weathering. *Annals of the Association of American Geographers*, 85, 38–64.

Reed, S.J.B. (1993) *Electron microprobe analysis*, 2nd edition. Cambridge University Press: Cambridge.

Royse, C.F., Sheridan, M.F. & Peirce, H.W. (1971) Geologic guidebook 4—highways of Arizona Arizona Highways 87, 88, and 188. *Arizona Bureau of Mines Bulletin*, 184, 1–66.

Ruxton, B.P. (1958) Weathering and subsurface erosion in granite at the piedmont angle, Balos, Sudan. *Geological Magazine*, 95(5), 353–377. Available from: https://doi.org/10.1017/S0016756800062944

Sales, J.K. (1968) Crustal mechanics of cordilleran foreland deformation: a regional and scale-model approach. *American Association of Petroleum Geologists Bulletin*, 52, 2016–2044.

Sari, M. (2021) Secondary toppling failure analysis and optimal support design for ignimbrites in the Ihlara Valley (Cappadocia, Turkey) by finite element method (FEM). *Geotechncal Geological Engineering*, 39(7), 5135–5160. Available from: https://doi.org/10.1007/s10706-10021-01819-10707

Sari, M. (2022) Evaluating rockfalls at a historical settlement in the Ihlara Vlley (Cappadocia, Turkey) using kinematic numerical 2D trajectory and risk rating methods. *Journal of Mountain Science*, 19(12), 3346–3369. Available from: https://doi.org/10.1007/s11629-022-7412-8

Sarikaya, M.A., Ciner, A. & Zreda, M. (2015) Fairy chimney erosion rates on Cappadocia ignimbrites, Turkey: insights from cosmogenic nuclides. *Geomorphology*, 234, 182–191. Available from: https://doi.org/10.1016/j.geomorph.2014.12.039

Scoon, R. (2013) The Cappadocia Word Heritage Site Turkey: active erosion of volcanic landscapes and ancient civilizations. *Geotravellers*, 2(41–45), 313–326.

Seaward, M.R.D. (1988) Lichen damage to ancient monuments: a case study. *The Lichenologist*, 20(3), 291–295. Available from: https://doi.org/10.1017/S0024282988000325

Self, S., Heiken, G., Sykes, M.L., Wohletz, K., Fisher, R.V. & Dethier, D.P. (1996) Field excursions to the Jemez Mountains, New Mexico. *New Mexico Bureau of Mines and Mineral Resources Bulletin*, 134, 1–72. Available from: https://doi.org/10.58799/B-134

Self, S., Randolph-Flagg, N., Bailey, J.E. & Manga, M. (2022) Exposed columns in the Valles Caldera ignimbrites as records of hydrothermal cooling, Jemez Mountains, New Mexico, USA. *Journal of Volcanology and Geothermal Research*, 426, 107536. Available from: https://doi.org/10.1016/j.jvolgeores.2022.107536

Seong, Y.B., Dorn, R.I. & Yu, B.Y. (2016) Evaluating the life expectancy of a desert pavement. *Earth-Science Reviews*, 162, 129–154. Available from: https://doi.org/10.1016/j.earscirev.2016.08.005

Seong, Y.B., Larson, P.H., Dorn, R.I. & Yu, B.Y. (2016) Evaluating process domains in small granitic watersheds: case study of Pima Wash, South Mountains, Sonoran Desert, USA. *Geomorphology*, 255, 108–124. Available from: https://doi.org/10.1016/j.geomorph.2015.12.014

Sherrod, D.R. & Tosdal, R.M. (1991) Geologic setting and Tertiary structural evolution of southwestern Arizona and southeastern California. *Journal of Geophysical Research - Solid Earth*, 96(B7), 12407–12423. Available from: https://doi.org/10.1029/90JB02688

Shtober-Zisu, N., Amasha, H. & Frumkin, A. (2017) Inland notches: lithological characteristics and climatic implications of subaerial cavernous landforms in Israel. *Earth Surface Processes and Landforms*, 42(12), 1820–1832. Available from: https://doi.org/10.1002/esp.4135

Skotnicki, S.J. & Ferguson, C.A. (1995) Geological map of the Goldfield quadrangle and the northern part of the Superstition Mountains SW quadrangles, Maricopa and Pinal Counties, Arizona. Arizona Geological Survey Open File Report 95-9. 1–26.

Sparavigna, A.C. (2011) Fairy chimneys in Peru. *Physics/Geophysics*. Available from: https://arxiv.org/pdf/1109.6617.pdf

Stuckless, J.S. & Sheridan, M.F. (1971) Tertiary volcanic stratigraphy in the Goldfield and Superstition Mountains, Arizona. *Geological Society of America Bulletin*, 82(11), 3235–3240. Available from: https://doi.org/10.1130/0016-7606%281971%2982%5B3235:TVSITG%5D2.0.CO;2

Topal, T. & Doyuran, V. (1997) Engineering geological properties and durability assessment of the Cappadocian tuff. *Engineering Geology*, 47, 175–187.

Twidale, C.R. (1974) Role of subterranean water in landform development in tropical and subtropical regions. In: LaFleur, R.G. (Ed.) *Groundwater as a geomorphic agent*. Boston: Allen and Unwin, pp. 91–134.

Twidale, C.R. (1990) The origin and implications of some erosional landforms. *The Journal of Geology*, 98(3), 343–364. Available from: https://doi.org/10.1086/629409

Twidale, C.R. (2002) The two-stage concept of landform and landscape development involving etching: origin, development and implications of an idea. *Earth Science Reviews*, 57(1-2), 37–74. Available from: https://doi.org/10.1016/S0012-8252(01)00059-9

Twidale, C.R. & Campbell, E.M. (1992) On the origin of pedestal rocks. *Zeitschrift fur Geomorphology N.F.*, 36(1), 1–13. Available from: https://doi.org/10.1127/zfg/36/1992/1

Twidale, C.R. & Mueller, J.E. (1988) Etching as a process of landform development. *The Professional Geographer*, 40(4), 379–391. Available from: https://doi.org/10.1111/j.0033-0124.1988.00379.x

UNESCO. (2022) Göreme National Park and the Rock Sites of Cappadocia. Available from: https://whc.unesco.org/en/list/357/. Accessed 24 June.

Valjarevic, A., Sreckovic-Batocanin, D., Zivkovic, D. & Peric, M. (2015) GIS analysis of dissipation time of landcape in the Devil's city (Serbia). *Actia Montanistica Slovaca*, 20(2), 148–155.

Viles, H.A. & Goudie, A.S. (2004) Biofilms and case hardening on sandstones from Al-Quawayra, Jordan. *Earth Surface Processes and Landforms*, 29(12), 1473–1485. Available from: https://doi.org/10.1002/esp.1134

Wahrhaftig, C. (1965) Stepped topography of the Southern Sierra Nevada. *Geological Society of America Bulletin*, 76(10), 1165–1190. Available from: https://doi.org/10.1130/0016-7606%281965%2976%5B1165:STOTSS%5D2.0.CO;2

Waters, A.C. (1966) Stein's Pillr area, central Oregin. *The Ore Bin*, 28(8), 137–150.

Wohletz, K. (2006) Fractures in welded tuff. *Geological Society of America Special Paper*, 408, 17–31.

Yakar, M. & Yilmaz, H.M. (2011) Determination of erosion on a small fairy chimney. *Experimental Techniques*, 2011(September/October), 76–82. Available from: https://doi.org/10.1111/j.1747-1567.2010.00661.x

Yilmaz, H.M., Yakar, M., Yildiz, F., Karabork, H., Kavurmaci, M.M., Mutluoglu, O. et al. (2009) Monitoring of corrosion in fairy chimney by terrestrial laser scanning. *Journal of International Environmental Application & Science*, 4, 86–91.

Yonkee, W.A. & Weil, A.B. (2015) Tectonic evolution of the Sevier and Laramide belts within the North American Cordillera orogenic system. *Earth-Science Reviews*, 150, 531–593. Available from: https://doi.org/10.1016/j.earscirev.2015.08.001